Sensor and Simulation Notes
Note

(Radiation Laboratory Report No. 010748-1-T)

March 1972

MODIFIED BICONICAL ANTENNAS

T.B.A. Senior and G.A. Desjardins

The University of Michigan Radiation Laboratory
Department of Electrical Engineering
Ann Arbor, Michigan 48105

Abstract

The early time behavior of the fields radiated by two types of EMP antennas is investigated. The first type is a bicone-cylinder in which each cone is mated directly to a semi-infinite cylinder of constant radius, thereby creating a ring discontinuity in slope at the junction. The second assumes a continuation of the bicone which matches the slope at the junction with the cone, producing there a ring discontinuity in curvature. Using geometrical diffraction theory techniques and knowing the diffraction matrices for the two forms of surface singularity, a high frequency asymptotic development of the radiated field is obtained for each antenna. Application of an inverse Fourier transform then yields a time domain solution valid for sufficiently early times. The solutions are computed and their validity investigated. Examples are given showing the reduction in the perturbation of the early time response associated with the smoother geometry.

1. Introduction

From an electromagnetic viewpoint the infinite biconical antenna is an ideal device for radiating an EMP. Since a constant voltage applied across the infinitesimal gap separating the two halves of the bicone produces a pure frequency-independent spherical TEM wave, a voltage pulse will create a radiating pulse which is identical in all respects. Unfortunately, such an antenna is unrealistic because of its infinite dimensions parallel and perpendicular to the axis of symmetry. A compromise which seeks to retain some of the electromagnetic advantages of the bicone whilst making the transverse dimensions finite is to mate each half of the bicone to some other geometrical structure at a selected distance from the gap. By choosing this structure to be a semi-infinite circular cylinder, we arrive at the bicone-cylinder studied by Sancer and Varvatsis (1971) and characterized by a slope discontinuity at the join. Within the spatial region which is directly illuminated, it is expected that the dominant contribution will still be the undistorted pulse radiated by the gap, but because of diffraction at the joins and the multiple interactions of these diffracted pulses with the rest of the antenna, the net field will be affected, with the short time perturbations being attributable to the diffraction of the high frequency components. Any modification in the cylindrical structure beyond the join will have a dominant effect on the field within the shadowed region which is entirely diffractive in nature, and can also distort yet further the field in the illuminated region through back reflection. On the semi-infinite cylinder, however, the surface field is primarily a traveling or surface wave excited by the join. If this were attenuated by progressive loading of the surface, the cylinder could then be terminated without further affect on the field in the illuminated region. Only on such a premise would an exact analysis of an infinite bicone-cylinder be relevant to a realistic antenna, and we must emphasize that the relevance would not extend to the deep shadowed regions of space.

The right circular cylinder is only one type of continuation structure for the bicone, and an infinity of other continuations are possible which also serve to limit the transverse dimension of the resulting antenna. One class of these produces

a smoother transition between the bicone and the continuation by matching the slope whilst leaving the curvature discontinuous at the join, and still higher order matching could be entertained. Such smoothing of a surface singularity reduces the high frequency diffraction, implying that a change from a slope discontinuity (in the first derivative of the profile) to a curvature discontinuity (in the second derivative of the profile) will decrease the perturbation of the direct radiated pulse for at least some span of elapsed time. Since the precise leading term in a high frequency asymptotic expansion of the diffraction coefficient for a line discontinuity in curvature has recently been obtained (Senior, 1971), it is now possible to quantify this effect. This is the purpose of the present Note.

We here examine the consequences as regards the early time behavior of the radiated field of replacing a cylindrical continuation of the bicone by a hyperbolic continuation so chosen as to remove the discontinuity in slope at the junction. The procedure that is adopted is to calculate the leading (first order) term in the high frequency expansion of the diffracted field at any arbitrary point in the illuminated region for each of the two geometries. The time domain solution for a step function voltage applied across the gap is then obtained by an inverse Fourier transformation. Although the range of elapsed times for which this solution is valid cannot be stated with any real certainty, an upper bound is available from a consideration of those ray interactions which are ignored in the frequency domain analysis. Not surprisingly, at every point in space there is some range of elapsed time for which the perturbation of the undistorted pulse is smaller when the discontinuity is in curvature rather than slope. Data are presented illustrating this effect and some general conclusions are drawn, but whether the improvement is sufficient to outweigh the disadvantages of this new geometry is a question beyond the scope of this Note.

These disadvantages are two-fold: increased difficulty of construction to produce the smooth junction and an increase in the overall diameter of the antenna. For any smooth and monotonic continuation, the maximum radius necessarily exceeds the radius of the join, and for the hyperbolic profile assumed in the analysis, the discontinuity in radius of curvature is proportional to the fractional

increase in maximum radius on changing from a cylindrical continuation (slope discontinuity). Indeed, this fractional increase is one of the key parameters in the final presentation of our results, but in practice it should be possible to obtain the advantages of the smoother geometry with a smaller increase. The only portion of the continuation structure which is essential to the analysis is that which is just beyond the join. The surface field here is basically a creeping wave whose strength and attenuation are known (Weston, 1965; Hong and Weston, 1966). Because of this attenuation, the requirements on loading to permit ultimate termination will be less stringent than was the case for a cylindrical continuation, and at some point of the curved surface beyond the join it would be acceptable to change to another surface profile more nearly approximating that of a right circular cylinder. The hyperbolic geometry would then apply only to a transition region between the bicone and the structure further out, and provided the second surface discontinuity was well within the shadow, its presence should have no effect on the field within the illuminated region, certainly as regards the early time behavior. However, these are practical considerations which are irrelevant to the main thrust of our analysis.

2. Preliminary Considerations

2.1 The Infinite Biconical Antenna

The antennas to be explored are all geometrical modifications of the infinite biconical antenna and it is therefore appropriate to consider first the field radiated by such an antenna when excited by a point generator at the apex of the cones.

The geometry is now as shown in Fig. 1. If (r, θ, ϕ) are spherical polar coordinates referred to an orgin at the apex, the field radiated by a time harmonic voltage generator of circular frequency $\omega = kc$ is

$$\underline{E} = \hat{\theta} \frac{A(\omega)}{r \sin\theta} e^{ik(r-ct)}, \qquad \underline{H} = \hat{\phi} \frac{YA(\omega)}{r \sin\theta} e^{ik(r-ct)} \tag{1}$$

in which

$$A(\omega) = \frac{Z}{2\pi} I(\omega, 0)$$

where $Z = 1/Y$ is the intrinsic impedance of free space and $I(\omega, 0)$ is the total surface current entering the upper cone from the generator at $r = 0$.

Knowing the structure of the field, we can integrate E_θ along the field line r = constant, ϕ = constant from the value $\theta = \theta_0$ appropriate to the upper cone to the value $\theta = \pi - \theta_0$ at the lower cone to obtain

$$V(\omega, r) = I(\omega, r) Z_c$$

where

$$Z_c = \frac{Z}{\pi} \ell n \left(\cot \frac{\theta_0}{2} \right)$$

is the characteristic impedance of the antenna. In particular, at $r = 0$

$$V(\omega) = I(\omega, 0) Z_c$$

where $V(\omega) = V(\omega, 0)$ is the strength of the voltage source, and if we now write

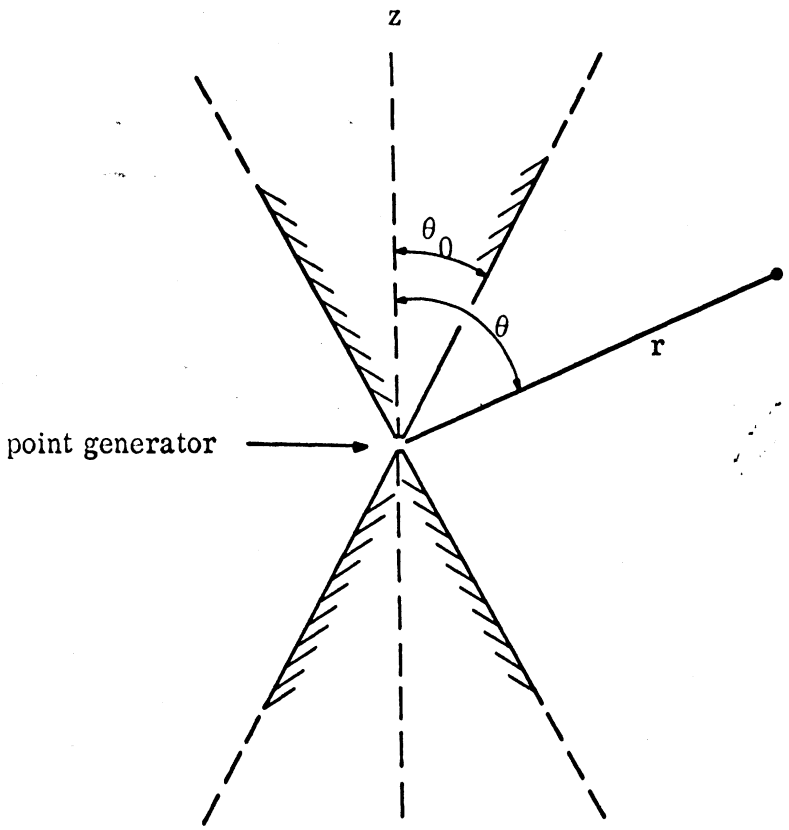

FIG. 1: INFINITE BICONICAL ANTENNA.

$$f_0 = \left\{2\ell n\left(\cot\frac{\theta_0}{2}\right)\right\}^{-1} , \tag{2}$$

we have

$$A(\omega) = V(\omega)f_0 . \tag{3}$$

The radiation field (1) is independent of ϕ and entirely specified by the θ component of the electric field, viz.

$$E_\theta = \frac{V(\omega)f_0}{r\sin\theta}\, e^{ik(r-ct)} . \tag{4}$$

Moreover, it is a function of frequency only through the phase factor and the frequency dependence of the excitation voltage. It therefore follows that if the excitation is the voltage pulse v(t), it will radiate undistorted except for the amplitude scaling factor $f_0/(r\sin\theta)$, and in particular, if v(t) is the unit (or Heaviside) step function U(t), then

$$E_\theta = \frac{f_0}{r\sin\theta}\, U(t-\frac{r}{c}) . \tag{5}$$

We shall henceforth restrict ourselves to such a voltage pulse.

2.2 Fourier Transform Relations

For the modified antenna geometries discussed in Section 2.3 the procedure that we shall follow is to develop first a high frequency asymptotic expansion of the radiated field for a simple harmonic source at the apex of the cones. In the illuminated region the leading term in the expansion is the field (4) appropriate to an infinite biconical antenna. The higher order terms are attributable to diffraction at the surface singularities, and to the accuracy that this expansion can be found, these terms are of the form

$$V(\omega)\omega^{-n-\frac{1}{2}}\, e^{ik(\ell-ct)}$$

for $n = 0, 1$, where ℓ is some distance. The early time behavior of the radiated field is then obtained by applying an inverse Fourier transform to each individual term with $V(\omega)$ as the spectrum of the unit step source voltage.

To permit the rigorous Fourier transformation of functions $f(t)$ which do not tend to zero as $t \to \infty$, it is necessary to assume that ω has a small positive imaginary part ϵ. With this extended definition, the Fourier transform of $f(t)$ is

$$\mathfrak{F}\{f(t)\} = F(\omega) = \int_{-\infty}^{\infty} e^{i\omega t} f(t)dt \tag{6}$$

and the inverse transform is

$$\mathfrak{F}^{-1}\{F(\omega)\} = f(t) = \frac{1}{2\pi} \int_{-\infty+i\epsilon}^{\infty+i\epsilon} e^{-i\omega t} F(\omega)d\omega \tag{7}$$

If $f(t)$ is the unit step function $U(t)$, direct integration shows that

$$F(\omega) = i/\omega \ .$$

Moreover, $\mathfrak{F}^{-1}\{F(\omega)\}$ can now be evaluated unambiguously, implying

$$U(t) = \frac{1}{2\pi} \int_{-\infty+i\epsilon}^{\infty+i\epsilon} \frac{i}{\omega} e^{-i\omega t} d\omega \ . \tag{8}$$

Consider $\mathfrak{F}^{-1}\{\omega^{-1/2}\}$, where the cut originating at the branch point $\omega = 0$ is assumed to lie along the negative real ω axis. If $t < 0$, the path of integration can be closed by the addition of a semi-circle of large radius in the upper half ω plane and the transform shown equal to zero. If $t > 0$, the addition of a semi-circle in the lower half plane reduces the transform to the sum of integrals along both sides of the cut, and these can be evaluated trivially. Hence

$$\mathfrak{F}^{-1}\left\{\omega^{-1/2}\right\} = (\pi t)^{-1/2} e^{-i\pi/4} U(t) .$$

Integration by parts now yields the two results which are needed in the sequel, viz.

$$\mathfrak{F}^{-1}\left\{i\omega^{-3/2} e^{ik\ell}\right\} = 2\pi^{-1/2} e^{-i\pi/4}\left(t-\frac{\ell}{c}\right)^{1/2} U\left(t-\frac{\ell}{c}\right) \tag{9}$$

and

$$\mathfrak{F}^{-1}\left\{i\omega^{-5/2} e^{ik\ell}\right\} = -\frac{4\pi^{-1/2}}{3} e^{i\pi/4}\left(t-\frac{\ell}{c}\right)^{3/2} U\left(t-\frac{\ell}{c}\right) , \tag{10}$$

which are special cases of the general formula

$$\mathfrak{F}^{-1}\left\{i\omega^{-n-\frac{1}{2}} e^{ik\ell}\right\} = \pi^{-1/2}\frac{(n-1)!}{(2n-1)!}\left\{4e^{-i\pi/2}\left(t-\frac{\ell}{c}\right)\right\}^{n-\frac{1}{2}} U\left(t-\frac{\ell}{c}\right) \tag{11}$$

valid for positive integer n.

2.3 Specific Geometry

In the region adjacent to the gap the antenna is assumed to be a bicone of half-cone angle θ_0, extending out to a radius $d\sin\theta_0$ where d is the slant length of the cone. At this point the profile is changed, and if ρ, z are cylindrical coordinates with origin at the gap and z axis coincident with the axis of symmetry, the requirements on the new profile $\rho = \rho(z)$ are that it be an analytic, monotonic function of z with $\rho \rightarrow$ finite limit as $z \rightarrow \infty$ and

$$\left.\begin{aligned} \rho &= d\sin\theta_0 \\ \frac{d\rho}{dz} &= \tan\theta_0 \end{aligned}\right\} \text{ at } z = d\cos\theta_0 .$$

Since the entire configuration is symmetrical about the plane $z = 0$, it is sufficient to consider only the upper cone and its continuation.

The most simple function having the above properties is a hyperbola, and we therefore choose the hyperbolic profile

$$\rho - d\sin\theta_0 = B\tan\theta_0 \left\{1 - \frac{B}{z - d\cos\theta_0 + B}\right\} \quad , \tag{12}$$

for $z \geq d\cos\theta_0$, where B is some constant yet to be chosen. At the junction with the upper cone, $\rho = d\sin\theta_0$ and $d\rho/dz = \tan\theta_0$, as required, and the (inward) curvature in any plane containing the z axis is

$$a_1 = \frac{1}{B}\sin 2\theta_0 \cos\theta_0 \ .$$

This is the quantity which determines the strength of the field diffracted at the junction of the bicone and its continuation.

It only remains to express B in terms of a convenient geometrical quantity natural to the problem. For this purpose, we note that as $z \to \infty$, $\rho \to d\sin\theta_0 + B\tan\theta_0$. Let us therefore write

$$\lim_{z \to \infty} \rho = d(1+\epsilon)\sin\theta_0 \tag{13}$$

where ϵ is the fractional increase in the overall radius of the antenna on changing from a circular cylindrical continuation of the bicone to a slope matching one. Then

$$B = \epsilon d\cos\theta_0$$

and

$$a_1 = \frac{1}{\epsilon d}\sin 2\theta_0 \tag{14}$$

with $\epsilon = 0$ implying a slope discontinuity at the junction.

3. Ray Techniques

The procedure that we shall follow in analyzing the transient radiation from the antenna is to first develop a high frequency asymptotic expansion for the field radiated when the voltage across the gap is a simple harmonic one with time variation $e^{-i\omega t}$. The only effective method for doing so is to use the geometrical theory of diffraction (GTD) originated by Keller (1957, 1962). The theory is basically an extension of geometrical optics to include the concept of diffracted rays produced by surface singularities, and since we shall re-phrase slightly the formulae of GTD to emphasize still more the similarity to geometrical optics, it is convenient to begin with a general survey of such aspects of ray techniques as are appropriate to a problem such as this.

3.1 An Overview

In geometrical optics the propagation of energy between two points Q and P occurs according to Fermat's principle that the optical distance between Q and P must be stationary with respect to small variations in path. In particular, therefore, the optical rays in a homogeneous isotropic medium are straight lines. The variation of intensity of the geometrical optics field along a ray is dictated by energy conservation: the energy flux in a tube of rays must be the same at all points along the tube.

Let us consider the vector case, and specifically the electric field $\underline{E}$. With reference to Fig. 2 we have that

$$\left|\underline{E}(P)\right| = \left|\underline{E}(Q)\right| \sqrt{\frac{dS_Q}{dS_P}}$$

where dS_Q and dS_P are the cross sections of the elementary tube of rays at Q and P respectively, and are inversely proportional to the Gaussian curvature of the wavefront. Thus, if we denote by s the oriented distance of the observation point P from a fixed origin Q, and by $\rho_1 = AQ$ and $\rho_2 = BQ$ the distances of the astigmatic lines A and B from Q, then since the polarization is unchanged

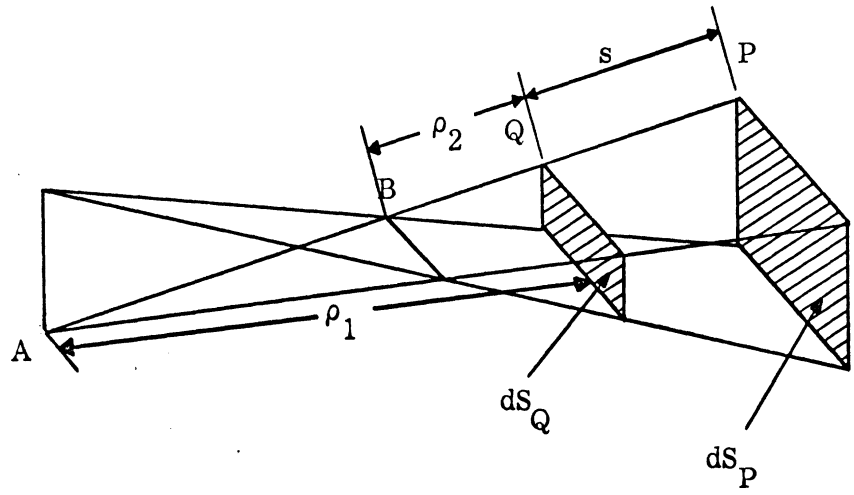

FIG. 2: ASTIGMATIC TUBE OF RAYS.

along the ray,

$$\underline{E}(P) = \underline{E}(Q)\,\Gamma e^{ik(s-ct)} \tag{15}$$

where

$$\Gamma = \sqrt{\left(\frac{\rho_1}{\rho_1+s}\right)\left(\frac{\rho_2}{\rho_2+s}\right)} \tag{16}$$

is the so-called divergence factor which is a measure of the spreading of the elementary tube of rays from Q to P.

Equation (15) yields an infinite value for the field at the caustics A and B where either $s = -\rho_1$ or $s = -\rho_2$, implying $\Gamma = \infty$. This is a universal failure of any ray technique and a procedure for obtaining a finite, frequency-dependent expression for the field in the vicinity of a caustic has been discussed by Kay and Keller (1954). However, on following a ray through a caustic and beyond, Γ is again finite, and provided we interpret $\sqrt{-1}$ as -i, Eq. (16) does predict the known phase delay of $\pi/2$ on passing through a line caustic in a positive direction.

At the surface of a body or, indeed, at any surface of discontinuity in a medium, the direction and wavefront curvature associated with any ray change discontinuously, as do the field strength and polarization. There are now two distinct cases depending on the principal radii of curvature of the surface at the point Q where the incident ray strikes. If both radii are non zero then, in the high frequency limit, the incident ray will produce a single reflected ray whose orientation is in accordance with Snell's laws of reflection at a plane interface. This is the geometrical optics situation and the strength of the reflected field at the surface is specified by the Fresnel reflection coefficients for plane wave incidence on a plane interface. A general expression for $\underline{E}^r(Q)$ has been derived by Fock (1965), and can be written most compactly as

$$\underline{E}^r(Q) = \bar{\bar{R}} \cdot \underline{E}^i(Q) \tag{17}$$

where the tensor reflection coefficient $\bar{\bar{R}}$ is a function of the angle of incidence and the electromagnetic parameters of the surface. For a perfectly conducting body, $\bar{\bar{R}}$ is such that $\hat{n} \wedge \underline{E}^r = -\hat{n} \wedge \underline{E}^i$ and $\hat{n} \cdot \underline{E}^r = \hat{n} \cdot \underline{E}^i$, where $\hat{n}$ is a unit vector normal.

To calculate the field on the reflected ray at a point P which is away from the surface we can again use Eq. (15) where ρ_1 and ρ_2 are now the principal radii of curvature of the reflected wavefront at the point of reflection, Q. In general, these depend on the angle of incidence, α, measured with respect to the local normal, the radii of curvature, s_1 and s_2, of the incident wavefront at Q, measured in and perpendicular to the plane of incidence respectively, and the corresponding radii, r_1 and r_2, of the surface at Q. As shown by Fock (1965) and Senior (1972),

$$\frac{1}{\rho_1} = \frac{1}{s_1} + \frac{2\sec\alpha}{r_1} \quad , \qquad \frac{1}{\rho_2} = \frac{1}{s_2} + \frac{2\cos\alpha}{r_2} \quad . \tag{18}$$

Observe that s_1, s_2 and r_1, r_2 are not necessarily principal radii of curvature. Indeed, if s_1' and s_2' are the principal radii for the incident wavefront at Q and β is the angle between the plane of s_1' and the plane of incidence,

$$\frac{1}{s_1} = \frac{\cos^2\beta}{s_1'} + \frac{\sin^2\beta}{s_2'} \quad , \qquad \frac{1}{s_2} = \frac{\sin^2\beta}{s_1'} + \frac{\cos^2\beta}{s_2'} \quad , \tag{19}$$

and a similar pair of formulae hold for the surface curvatures.

The second case to be considered is that in which one or both of the principal radii of curvature are zero at the point Q, corresponding to a line or point (vertex) singularity respectively. Although geometrical optics is no longer applicable, geometrical diffraction theory now takes over, and each incident ray produces an infinity of diffracted rays. For the purposes of the present problem, only the line singularity is important. This may be produced by a discontinuity in the first derivative of the surface (wedge-like singularity) or in some higher derivative, the earlier ones being continuous at Q, but in either case the diffracted

rays are confined to the surface of the Keller cone. In the immediate vicinity of Q the field on any one diffracted ray is entirely a local property of the surface at Q, and can be found by solving a canonical problem displaying the geometry in question. In principal at least, this enables us to relate the reflected field strength at a point close to Q to the incident field strength via an equation similar to (17) in which a tensor diffraction coefficient takes the place of $\overline{\overline{R}}$.

Unfortunately we now run into a conceptual difficulty in trying to find the diffracted field at a remote point P along a diffracted ray. Since the surface singularity is a caustic for the diffracted ray tube in a plane perpendicular to the singularity, we cannot use the divergence factor (16) to proceed outwards from Q. For this reason, it has become customary (following Keller, 1957) to omit any explicit statement of a diffraction tensor for points close to Q, and to proceed immediately to a "remote" point P distance s ($>>\lambda$) from Q, writing the diffracted field there as

$$\underline{E}^d(P) = \sqrt{\frac{\rho_1}{\rho_1 + s}}\ \frac{e^{i\pi/4}}{\sqrt{2\pi k s}}\ e^{ik(s-ct)}\ \overline{\overline{D}} \cdot \underline{E}^i(Q) \qquad (20)$$

where ρ_1 is the transverse radius of curvature of the diffracted ray tube at Q. If β is the angle between the incident unit vector $\hat{u}$ and a tangent unit vector $\hat{\tau}$ along the singularity or "edge", the local radius of which is r_1, τ is arclength along the edge, $\hat{n}$ is the principal unit vector normal to the edge (i.e. pointing towards the center of curvature) and $\hat{s}$ is a unit vector in the direction of the diffracted ray, then

$$\rho_1 = \frac{r_1 \sin^2\beta}{(\hat{u} - \hat{s}) \cdot \hat{n} + r_1 \hat{\tau} \cdot (\partial \hat{u}/\partial \tau)} \qquad (21)$$

For a wedge-type singularity

$$\overline{\overline{D}} = -\operatorname{cosec}\beta\, \overline{\overline{\Delta}} \qquad (22)$$

where $\overline{\overline{\Delta}}$ is given by Senior and Uslenghi (1971) in terms of a set of surface-oriented base vectors.

Even if we grant that the above procedure is the most rigorously justifiable one, we can still enhance the similarity of the diffraction and reflection processes by regarding $\overline{\overline{D}}$ as a diffraction tensor which relates the field on a diffracted ray at a distance $s \gtrsim \lambda$ from Q to the incident field at Q. If this displaced point is denoted by Q', Eq. (20) can be decomposed into two equations analogous to (15) and (17), viz.

$$\underline{E}^d(Q') = \overline{\overline{D}} \cdot \underline{E}^i(Q), \tag{23}$$

$$\underline{E}^d(P) = \underline{E}^d(Q')\, \Gamma e^{ik(s-ct)} \tag{24}$$

where the divergence factor Γ has the standard form (16) with

$$\rho_2 = \frac{i}{2\pi k} \tag{25}$$

and the proviso that $\sqrt{i} = e^{i\pi/4}$. Thus

$$\Gamma = \sqrt{\left(\frac{\rho_1}{\rho_1 + s}\right)\left(\frac{i}{i + 2\pi k s}\right)} \tag{26}$$

and though Eqs. (23), (24) and (26) are no longer equivalent to (20) for $ks \lesssim 1$, for $ks \gg 1$ (the condition under which the diffraction tensor $\overline{\overline{D}}$ was originally deduced),

$$\Gamma \simeq \sqrt{\frac{\rho_1}{\rho_1 + s}}\, \frac{e^{i\pi/4}}{\sqrt{2\pi k s}} \quad , \tag{27}$$

and the equivalence is restored.

In a problem where both diffraction and reflection occur, the main advantage of the present interpretation is that we can treat the two processes similarly and proceed stepwise along all rays using the same general formula for Γ. But the advantages are not overwhelming, and one penalty that we do pay is that Γ can now involve the wave number, k.

3.2 Diffraction Tensors

The diffraction tensor for a line discontinuity in slope (wedge-like singularity) was originally developed by Keller (1957) and was put into a somewhat more general form by Senior and Uslenghi (1971). The analogous result for a line discontinuity in curvature was obtained by Senior (1971), and to present the tensors in the form implied by our preceding remarks, it is sufficient to take only a discontinuity in slope since the result for a discontinuity in curvature differs only in the replacement of one pair of parameters by another.

Consider a wedge-like singularity shown in Fig. 3. Let the interior half angle of the wedge be Ω and choose a base set of unit vectors $\hat{T}, \hat{N}, \hat{B}$ with $\hat{N}$ normal to the edge and pointing out, $\hat{B}$ binormal to the edge and pointing into the shadowed half space, and $\hat{T} = \hat{N} \wedge \hat{B}$ to make the system right-handed. Then if the incident ray direction is

$$\hat{i} = \hat{T}\cos\beta - \hat{N}\sin\beta\sin\alpha + \hat{B}\sin\beta\cos\alpha \tag{28}$$

with $-\pi/2+\Omega \leq \alpha \leq \pi/2$, $0 < \beta < \pi$ and the diffracted ray direction is

$$\hat{d} = \hat{T}\cos\beta + \hat{N}\sin\beta\sin\gamma - \hat{B}\sin\beta\cos\gamma \tag{29}$$

with $-\pi/2+\Omega \leq \gamma \leq 3\pi/2-\Omega$ (see Fig. 3), we have

$$\underline{E}^d(P) = \overline{\overline{D}} \cdot \underline{E}^i(P) \tag{30}$$

at any point P of the singularity where $\underline{E}^d(P)$ and $\underline{E}^i(P)$ are the diffracted and incident electric fields at P expressed as row and column vectors respectively in the base $\hat{T}, \hat{N}, \hat{B}$, and

$$\overline{\overline{D}} = -\frac{1}{\sin\beta}\begin{pmatrix} -(X-Y) & 0 & 0 \\ (X-Y)\cot\beta\sin\gamma & (X+Y)\cos\gamma\cos\alpha & (X+Y)\cos\gamma\sin\alpha \\ -(X-Y)\cot\beta\cos\gamma & (X+Y)\sin\gamma\cos\alpha & (X+Y)\sin\gamma\sin\alpha \end{pmatrix}$$

(Senior and Uslenghi, 1971, Appendix, with $\delta = 0$) where

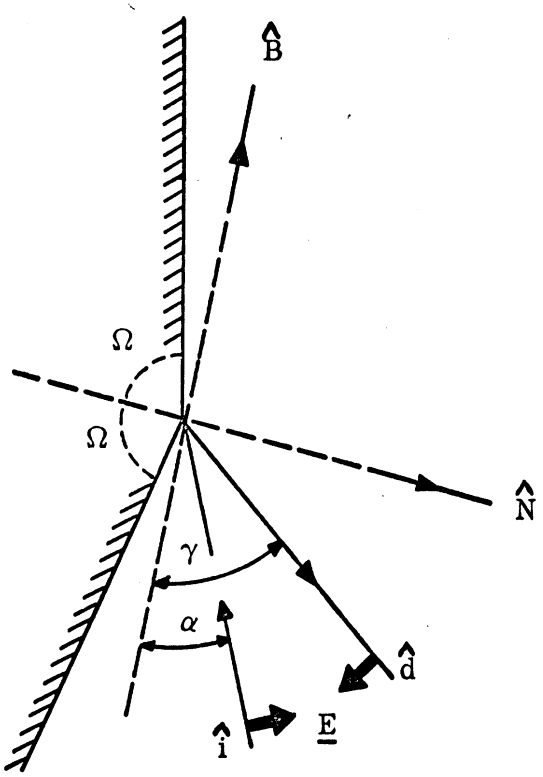

FIG. 3: GEOMETRY FOR A WEDGE-LIKE SINGULARITY.

$$X = \lambda \sin\lambda\pi \left\{ \cos\lambda\pi - \cos\lambda(\alpha - \gamma) \right\}^{-1} \tag{32}$$

$$Y = \lambda \sin\lambda\pi \left\{ \cos\lambda\pi + \cos\lambda(\pi - \alpha - \gamma) \right\}^{-1} \tag{33}$$

with

$$\lambda = \frac{1}{2\left(1 - \frac{\Omega}{\pi}\right)} \quad . \tag{34}$$

In the present problem the rotational symmetry implies that any ray incident on the singularity lies in the $\hat{N}, \hat{B}$ plane. Hence, $\beta = \pi/2$. Moreover, the incident electric vector also lies in this plane and, of necessity, is perpendicular to $\hat{i}$. We can therefore write

$$\underline{E}^{i}(P) = A(\hat{N}\cos\alpha + \hat{B}\sin\alpha)$$

where A is some constant, and when this is substituted into Eq. (30) we have

$$\underline{E}^{d}(P) = A(X+Y)\left\{-\hat{N}\cos\gamma - \hat{B}\sin\gamma\right\}$$

which is a vector perpendicular to $\hat{d}$. As regards the present problem we can now suppress entirely the vector characteristics of the diffraction process by adopting as a convention that the orientation of the electric vectors are as shown in Fig. 3. This allows us to replace the diffraction tensor $\overline{\overline{D}}$ by the scalar factor D where

$$D = X + Y \tag{35}$$

The situation is directly analogous to reflection at a metallic surface for which $\overline{\overline{R}}$ reduces to the scalar R = 1 for the electric vector orientations shown in Fig. 3.

If the surface singularity is a line discontinuity in curvature rather than slope the definitions of the base vectors $\hat{T}, \hat{N}, \hat{B}$ and the angles α, β, γ are identical to those given above, and the diffraction tensor differs from that in Eq. (31) only in having X and Y replaced by

$$\frac{a_1-a_2}{2ik}\,\frac{\sec^2\frac{\alpha-\gamma}{2}}{\cos\alpha+\cos\gamma}\quad,\qquad \frac{a_1-a_2}{2ik}\,\frac{\sec^2\frac{\alpha+\gamma}{2}}{\cos\alpha+\cos\gamma}$$

where a_1 and a_2 are the curvatures of the upper and lower surfaces, respectively, at the singularity. If the lower surface is planar, $a_2 = 0$.

For both the slope and curvature discontinuities, a case of particular interest to us is that in which the incident ray direction is along the lower planar face, i.e. $\alpha = -\frac{\pi}{2}+\Omega$ We then have

$$X = Y = \frac{\lambda \sin\lambda\pi}{\cos\lambda\pi+\cos\lambda\left(\frac{3\pi}{2}-\Omega-\gamma\right)}$$

and for a slope discontinuity the scalar diffraction coefficient for diffraction in a direction γ is

$$D^s = \frac{2\lambda \sin\lambda\pi}{\cos\lambda\pi+\cos\lambda\left(\frac{3\pi}{2}-\Omega-\gamma\right)} \quad . \tag{36}$$

The analogous result for a curvature discontinuity with $a_2 = 0$ is

$$D^c = \frac{2a_1}{ik}\,\frac{1+\sin\Omega\cos\gamma}{(\sin\Omega+\cos\gamma)^3} \quad . \tag{37}$$

With the approach that we have adopted, a factor proportional to $k^{-1/2}$ has been absorbed into the divergence coefficient for a line singularity, leaving D^s independent of frequency. By comparison D^c is smaller by a factor k^{-1}, showing the reduced influence of a curvature discontinuity at high frequencies. In both cases, however, the expression given is only the leading term in a high frequency asymptotic expansion, with the next term being smaller by a factor k^{-1}, and since these higher order terms cannot be obtained by a purely local analysis, their inclusion is beyond the scope of any analysis such as this.

3.3 Limitations

Let us now examine the implications of ray techniques as regards the derivation of a valid estimate for the field radiated by the antenna. Although we

shall obtain the time domain solution by inverse Fourier transformation of the high frequency response, quite different factors influence the accuracies in the two domains.

In the frequency domain, the relative importance of individual contributions to the field is determined by the k dependence of their amplitudes. If the amplitude of a direct ray contribution from the source is A, where A is independent of k, that for a contribution singly diffracted at a slope discontinuity is $Ak^{-1/2}\{1+O(k^{-1})\}$. If a diffracted ray is subsequently reflected at a surface whose radii are large, the k dependence is unaffected, though it should be noted that the reflection coefficient is independent of k only to the leading order. On the other hand, a secondary diffraction at a slope discontinuity will reduce the amplitude to $Ak^{-1}\{1+O(k^{-1})\}$.

In the present problem it is possible for a ray to be diffracted back to the source and then re-radiated. It is intuitively obvious that the nature of this re-radiation (or re-diffraction) will depend on the impedance of the source as well as the geometry of the gap, but the factor which quantifies this process is quite unknown even in its k dependence. It is therefore necessary to exclude any such ray contribution from our analysis, and the consequences of this are unfortunate. at least from a rigorous viewpoint. If, for example, the factor were independent of k, the contribution of a re-radiated ray would be of the same order as that for a ray diffracted at a surface singularity, regardless of its nature, and this would invalidate all terms in the high frequency expansion beyond the first, corresponding to direct radiation from the source; it is not inconceivable that the factor could be proportional to $k^{1/2}$, which would invalidate even the leading term!

The validity of even a single term in the high frequency expansion of the field now rests on an assumption about the frequency dependence of the re-radiation factor. On the premise that any EMP antenna which did not produce an early time behavior of the radiated field comparable to that of the excitation voltage would have its gap configuration changed until it did, we shall henceforth assume that the re-radiation factor is proportional to some negative (perhaps fractional)

power of k, thereby reducing the importance of any such ray contribution below that of a single diffracted ray, but not below that of a double diffracted ray.* In consequence, the only contributions which can be entertained are those of the direct ray from the source and the rays singly diffracted at the surface discontinuities, either directly to the point of observation, or via an intermediate reflection off the sides of the bicone. The resulting expansion in the frequency domain is then

$$A + Bk^{-1/2}\{1 + O(k^{-\epsilon})\}$$

for a slope discontinuity, or

$$A + Bk^{-3/2}\{1 + O(k^{-\epsilon})\}$$

for a curvature discontinuity, where $\epsilon > 0$ and we have again omitted the phase factors produced by the different ray paths.

Let us now turn to the time domain. From a high frequency estimate of the field we can deduce the early time behavior of the transient response by inverse Fourier transformation, but the validity of the result is not without question. Whereas the lengths of the individual paths by which the ray contributions reach the field point are no direct concern in the frequency domain, they are vital in the time domain since these are reflected in time separations. The shortest ray path whose contribution is omitted now provides an upper bound on the elapsed time beyond which the time domain response is patently invalid. In the present problem the bound is provided by either the doubly diffracted ray or the re-radiated one, whichever is shorter, but even within this bound the accuracy of the solution is not entirely certain. Take, for example, a singly diffracted ray contribution. In the frequency domain, only the leading term in the asymptotic expansion of the diffraction coefficient was included in estimating the contribution, yet all terms

---

* For a surface discontinuity in curvature it is even less justifiable to include doubly diffracted rays since their contribution is $O(k^{-3})$ whereas the correction to a singly diffracted ray contribution is $O(k^{-5/2})$.

would yield some contribution in the time domain. Unfortunately, it is almost impossible to estimate the error resulting from the omission of these terms, and on a strictly mathematical basis there are difficulties in justifying the Fourier transformation of an asymptotic expansion in the first place.

4. Analysis

4.1 Frequency Domain

We shall now use the geometrical theory of diffraction to develop a high frequency expansion of the field radiated by the antenna. The contributions which will be included are those for rays singly diffracted at the surface singularities and which then reach the field point either directly or by reflection off the sides of the cone, plus the direct contribution from the source. Subject to the assumption about the re-radiation properties of the source referred to in the previous section, the resulting asymptotic expansion is accurate to the first two orders in k.

The polar coordinates of the field point P_0 are (r,θ) where θ $(\theta_0 < \theta \leq \pi/2)$ is measured with respect to the symmetry (z) axis of the antenna. For simplicity it will be assumed that P_0 is in the far field of the biconical portion, which allows us to treat as parallel all rays reaching P_0.

The procedure to be followed is the same whether the surface singularities are discontinuities in slope or curvature, and since the only difference between the formulae is in the expression for the diffraction coefficient D, it is sufficient to describe the analysis in terms of slope discontinuities. The geometry is now as shown in Fig. 4, where we have included the ray paths to be considered. Observe that because of the azimuthal symmetry of the problem, all rays reaching P are confined to a single plane through the z axis.

Let us begin by establishing some of the more important path lengths and angles associated with the rays shown in Fig. 4. The direct ray is OP_0, and $[OP_0] = r$ by definition. The two simple diffracted rays are OP_1P_0 and OP_2P_0. Since the interior half wedge angle Ω is

$$\Omega = \frac{1}{2}(\pi - \theta_0) \tag{38}$$

and $\angle P_1OP_0 = \theta - \theta_0$, the diffraction angle γ (see Fig. 3) for the upper path is

$$\gamma = \frac{3\pi}{2} - \Omega - \theta = \pi - \theta + \frac{\theta_0}{2} \ . \tag{39}$$

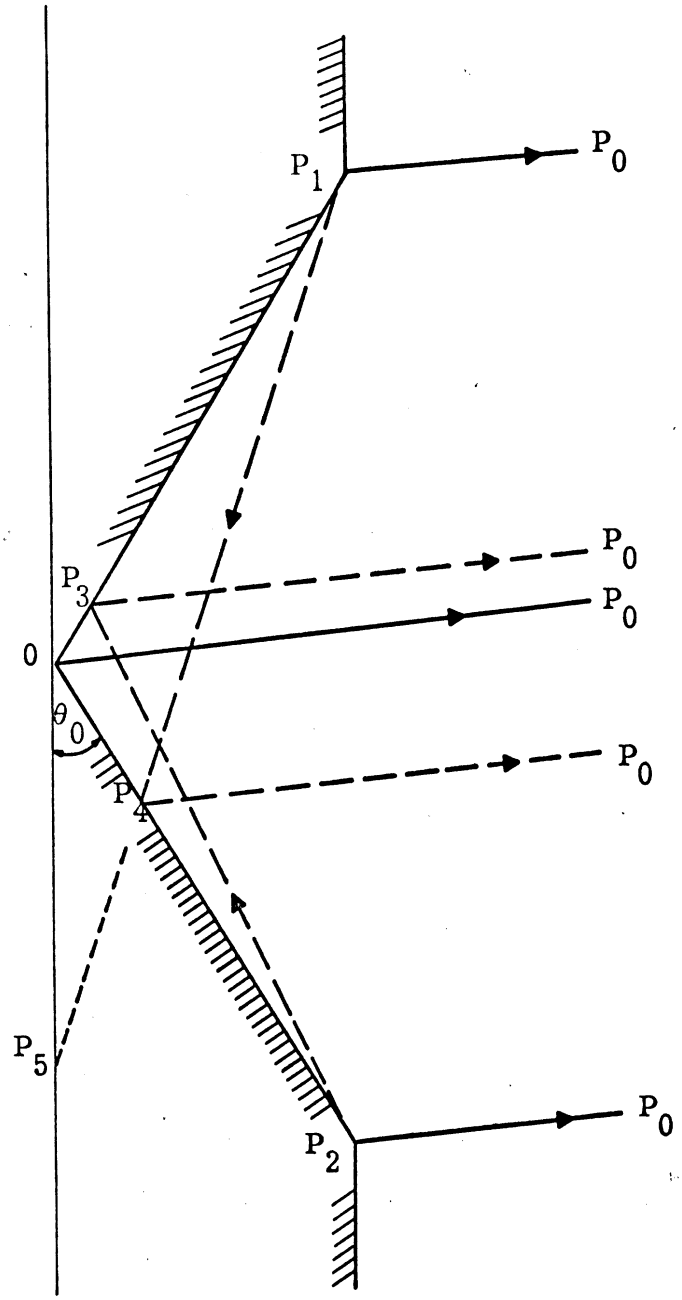

FIG. 4: THE GEOMETRY, SHOWING THE MORE IMPORTANT RAYS.

Also,

$$[P_1P_0] = r - [OP_1]\cos\angle P_1OP_0 = r - d\cos(\theta-\theta_0) \tag{40}$$

where d is the slant length of the cone. For the lower path OP_2P_0, the corresponding results can be obtained by replacing θ by $\pi-\theta$.

The two diffracted-reflected rays are $OP_1P_4P_0$ and $OP_2P_3P_0$. For the former, $\angle OP_4P_1 = \pi-\theta_0-\theta$ and hence $\angle OP_1P_4 = 3\theta_0+\theta-\pi$. If this path is to exist, it is necessary that

$$0 < 3\theta_0+\theta-\pi < \theta_0$$

where we have excluded the extremes for which the reflection point coincides with either the source O or the surface singularity P_2, and thus

$$\pi-3\theta_0 < \theta < \pi-2\theta_0 \tag{41}$$

showing that θ_0 must exceed $\pi/4$. The diffraction angle γ for this path is

$$\gamma = \frac{5\theta_0}{2}+\theta-\pi \ . \tag{42}$$

Moreover, from triangle OP_1P_4,

$$[P_1P_4] = \frac{d\sin 2\theta_0}{\sin(\theta+\theta_0)} \ , \qquad [OP_4] = \frac{d\sin(3\theta_0+\theta-\pi)}{\sin(\pi-\theta-\theta_0)} \tag{43}$$

and hence

$$[P_4P_0] = r - d\sin(\theta+3\theta_0)\cot(\theta+\theta_0) \tag{44}$$

implying

$$[OP_1]+[P_1P_4]+[P_4P_0] = r+d\{1-\cos(\theta+3\theta_0)\} \ . \tag{45}$$

For the other path the corresponding results can again be obtained by replacing θ by $\pi-\theta$. In particular, the criterion for existence of this path is

$$2\theta_0 < \theta < 3\theta_0 \ . \tag{46}$$

The next task is to determine the divergence factors associated with the various rays. For a ray OP_1 incident on the surface singularity P_1 and diffracted in a direction γ (see Fig. 3), the diffracted wavefront at P_1 has a radius of curvature in a plane perpendicular to the plane of incidence given by Eq. (21). In this formula,

$$\hat{u}\cdot\hat{n} = -\sin\theta_0 , \qquad \hat{s}\cdot\hat{n} = -\sin\left(\gamma - \frac{\theta_0}{2}\right) , \qquad \hat{\tau}\cdot\frac{\partial\hat{u}}{\partial\tau} = \frac{1}{d} ,$$

from which we obtain

$$\rho_1 = d\sin\theta_0 \operatorname{cosec}\left(\gamma - \frac{\theta_0}{2}\right) . \tag{47}$$

Hence, for the diffracted ray path OP_1P_0 for which γ is given by Eq. (39),

$$\rho_1 = d\sin\theta_0 \operatorname{cosec}\theta$$

and

$$\Gamma = \Gamma_{i10} \sim \frac{1}{r}\sqrt{\frac{d\sin\theta_0}{2\pi k\sin\theta}}\, e^{i\pi/4} , \tag{48}$$

in which the far field approximation has been made. For the ray diffracted towards P_4, the diffraction angle γ is given by (42). Thus

$$\rho_1 = -d\sin\theta_0 \operatorname{cosec}(\theta + 2\theta_0) . \tag{49}$$

At a distance s along this ray,

$$\Gamma = \left\{ s\left(1 - \frac{s}{d}\sin(\theta + 2\theta_0)\operatorname{cosec}\theta_0\right)\right\}^{-1/2} \frac{e^{i\pi/4}}{\sqrt{2\pi k}}$$

and the astigmatic nature of this tube of rays is obvious. Indeed, in a plane perpendicular to the plane of incidence at P_4, the radius of curvature of the incident wavefront is given by (49), corresponding to a caustic at P_5, whereas in the plane of incidence the caustic is at P_1. At the point P_4,

$$s = [P_1P_4] = \frac{d \sin 2\theta_0}{\sin(\theta+\theta_0)}$$

and

$$\Gamma = \Gamma_{i14} = \frac{\sin(\theta+\theta_0)}{\sqrt{2\pi kd \sin 2\theta_0 \sin(3\theta_0+\theta-\pi)}} e^{i\pi/4} \quad . \tag{50}$$

To find the principal radii of curvature ρ_1 and ρ_2 of the reflected wavefront at P_4, we need also the radii of curvature of the surface. In the plane of incidence the radius is clearly infinite. In the perpendicular plane through P_4, the (slant) section of the cone is an ellipse of major axis $[OP_4]\tan 2\theta_0$. Since the minor axis is $[OP_4]\tan 2\theta_0 \cos\theta_0$, the radius of curvature is

$$r_2 = \frac{1}{2}[OP_4]\tan 2\theta_0 \cos^2\theta_0$$

$$= d \frac{\sin(\theta+3\theta_0-\pi)\sin\theta_0 \cos^3\theta_0}{\sin(\theta+\theta_0)\cos 2\theta_0} \tag{51}$$

and hence, from the Eqs.(18),

$$\frac{1}{\rho_1} = \frac{1}{[P_1P_4]} + \frac{2\sec\alpha}{\infty} \quad ,$$

$$\frac{1}{\rho_2} = \frac{1}{-[P_4P_5]} + \frac{2\cos\alpha}{r_2}$$

with

$$\alpha = \theta+\theta_0 - \frac{\pi}{2} \quad ,$$

implying

$$\rho_1 = d \frac{\sin 2\theta_0}{\sin(\theta+\theta_0)} \quad , \tag{52}$$

$$\rho_2 = \frac{d}{4} \frac{\sin 2\theta_0 \cos^2\theta_0 \sin(3\theta_0+\theta-\pi)}{\sin(\theta+\theta_0)\left\{\sin(\theta+\theta_0)\cos 2\theta_0 - \frac{1}{2}\cos^3\theta_0 \sin(\theta+2\theta_0)\right\}} \quad . \tag{53}$$

The divergence factor for the reflected tube of rays is therefore

$$\Gamma = \Gamma_{140} \sim \frac{d}{2r} \frac{\sin 2\theta_0 \cos\theta_0}{\sin(\theta+\theta_0)} \sqrt{\frac{\sin(3\theta_0+\theta-\pi)}{\sin(\theta+\theta_0)\cos 2\theta_0 - \frac{1}{2}\cos^3\theta_0 \sin(\theta+2\theta_0)}} \tag{54}$$

in which the far field approximation has been made.

We can now start assembling the ray contributions to the radiated field at P_0. For the direct ray OP_0 from the source we have, from Eq. (1),

$$E(P_0) = \frac{A(\omega)}{r \sin\theta} e^{ik(r-ct)} \tag{55}$$

where the symbol E will be used throughout to denote the θ component of the electric field. For the diffracted ray OP_1P_0,

$$E(P_0) = E^i(P_1) D \Gamma_{i10} e^{ik([P_1P_0]-ct)} \quad . \tag{56}$$

Since the diffraction angle γ is given by Eq. (39), the diffraction coefficient D for a slope discontinuity is, from Eq. (36),

$$D^s(\theta) = \frac{2\lambda \sin\lambda\pi}{\cos\lambda\pi + \cos\lambda\theta} \tag{57}$$

with

$$\lambda = \left(1 + \frac{\theta_0}{\pi}\right)^{-1} \quad , \tag{58}$$

whereas for a curvature discontinuity,

$$D^c(\theta) = \frac{2a_1}{ik} \frac{1 - \cos\theta_0 \cos\left(\theta + \frac{\theta_0}{2}\right)}{\left\{\cos\theta_0 - \cos\left(\theta + \frac{\theta_0}{2}\right)\right\}^3} \tag{59}$$

from Eq. (37). For brevity we shall denote both $D^s(\theta)$ and $D^c(\theta)$ by the same symbol $D(\theta)$. Also,

$$E^i(P_1) = \frac{A(\omega)}{2d \sin\theta_0} e^{ik(d - ct)} \tag{60}$$

where the factor 2 appears because GTD requires only the incident rather than the total field arriving at a singularity, and at grazing incidence, the former is one-half of the latter. On inserting this expression into (56) and using (40) and (43), the contribution of the diffracted ray OP_1P_0 is found to be

$$E(P_0) \sim \frac{A(\omega)}{r \sin\theta} \frac{1}{2} \sqrt{\frac{\sin\theta}{2\pi kd \sin\theta_0}} D(\theta) e^{i\pi/4} e^{ik\{r + d - d\cos(\theta - \theta_0) - ct\}} . \tag{61}$$

The contribution of the diffracted ray OP_2P_0 differs only in having $\pi - \theta$ in place of θ.

For the diffracted-reflected ray $OP_1P_4P_0$,

$$E(P_0) = E^i(P_1) D \Gamma_{i14} e^{ik[P_1P_4]} R \Gamma_{140} e^{ik([P_4P_0] - ct)} . \tag{62}$$

Comparison of the diffraction angles (39) and (42) shows that

$$D \equiv D(2\pi - 2\theta_0 - \theta) .$$

Also, for a normal component of the electric field, R = 1. Hence, from Eqs. (45), (50), and (54), the contribution of this ray is

$$E(P_0) \sim \frac{A(\omega)\cos\theta_0}{4r}\sqrt{\frac{\cot\theta_0}{\pi kd\left\{\sin(\theta+\theta_0)\cos 2\theta_0 - \frac{1}{2}\cos^3\theta_0\sin(\theta+2\theta_0)\right\}}}\cdot$$

$$\cdot D(2\pi-2\theta_0-\theta)\, e^{i\pi/4} e^{ik\left\{r+d-d\cos(\theta+3\theta_0)-ct\right\}}. \quad (63)$$

Since the contribution of the ray $OP_2P_3P_0$ again differs only in having $\pi-\theta$ in place of θ, the far zone radiated field at P_0 correct to the first two orders of k is

$$E(P_0) \sim \frac{A(\omega)}{r\sin\theta} e^{ik(r-ct)}\left[1+\frac{1}{2}\sqrt{\frac{\sin\theta}{2\pi kd\sin\theta_0}}\, e^{\frac{i\pi}{4}+ikd}\left\{D(\theta)e^{-ikd\cos(\theta-\theta_0)}\right.\right.$$

$$+D(\pi-\theta)e^{ikd\cos(\theta+\theta_0)} + \nu_1 F(\theta)D(2\pi-2\theta_0-\theta)e^{-ikd\cos(\theta+3\theta_0)}$$

$$\left.\left.+\nu_2 F(\pi-\theta)D(\pi-2\theta_0+\theta)e^{ikd\cos(3\theta_0-\theta)}\right\}\right] \quad (64)$$

where

$$F(\theta) = \sqrt{\frac{\sin\theta\cos^3\theta_0}{2\sin(\theta+\theta_0)\cos 2\theta_0 - \cos^3\theta_0\sin(\theta+2\theta_0)}}. \quad (65)$$

In Eq. (64), $\nu_1 = 0$ unless

$$\pi-3\theta_0 < \theta < \pi-2\theta_0$$

when $\nu_1 = 1$, and $\nu_2 = 0$ unless

$$2\theta_0 < \theta < 3\theta_0$$

when $\nu_2 = 1$, with the additional restriction that $\theta_0 < \theta \leq \pi/2$. When normalized relative to the direct radiated field of the source, the perturbation field is therefore

$$\delta E(P_0) = \frac{1}{2}\sqrt{\frac{\sin\theta}{2\pi kd\sin\theta_0}}\, e^{\frac{i\pi}{4}} + ikd\Big[D(\theta)\, e^{-ikd\cos(\theta-\theta_0)} + D(\pi-\theta)e^{ikd\cos(\theta+\theta_0)}$$

$$+ \nu_1 F(\theta)D(2\pi - 2\theta_0 - \theta)\, e^{-ikd\cos(\theta+3\theta_0)} + \nu_2 F(\pi-\theta)D(\pi-2\theta_0+\theta)e^{ikd\cos(3\theta_0-\theta)}\Big] \quad . \tag{66}$$

which is $O(k^{-1/2})$ for a slope discontinuity, but $O(k^{-3/2})$ for a discontinuity in curvature.

The diffracted-reflected rays can only exist for restricted ranges of θ and to better appreciate when either or both of the last two terms in (64) and (66) are present, Fig. 5 shows the situations in which $\nu_1 = 1$ or $\nu_2 = 1$ for $\theta_0 < \pi/4$. Observe that neither reflected ray can occur if $3\theta_0 < \theta \leq \pi/2$ and that $\nu_1 = 0$ for all θ if $\theta_0 < \pi/6$.

4.2 Time Domain

For a voltage pulse applied across the gap, the early time behavior of the radiated field can be obtained by the inverse Fourier transformation of the asymptotic expansion (64) for $E(P_0)$. The particular source voltage that we shall consider is the unit step function U(t) for which (see Eq. 3)

$$A(\omega) = \frac{i}{\omega} f_0 \quad , \tag{67}$$

and the contribution to the field produced by direct radiation from the gap is

$$E(P_0) = \mathfrak{F}^{-1}\left\{\frac{i}{\omega} e^{i\omega r/c}\, \frac{f_0}{r\sin\theta}\right\}$$

$$= \frac{f_0}{r\sin\theta}\, U(t - \frac{r}{c}) \quad .$$

The diffracted and diffracted-reflected contributions then appear at times which are delayed by amounts proportional to the increase in path length.

To simplify the subsequent presentation of the data, it is convenient to take the origin of time at the instant at which the direct contribution arrives at

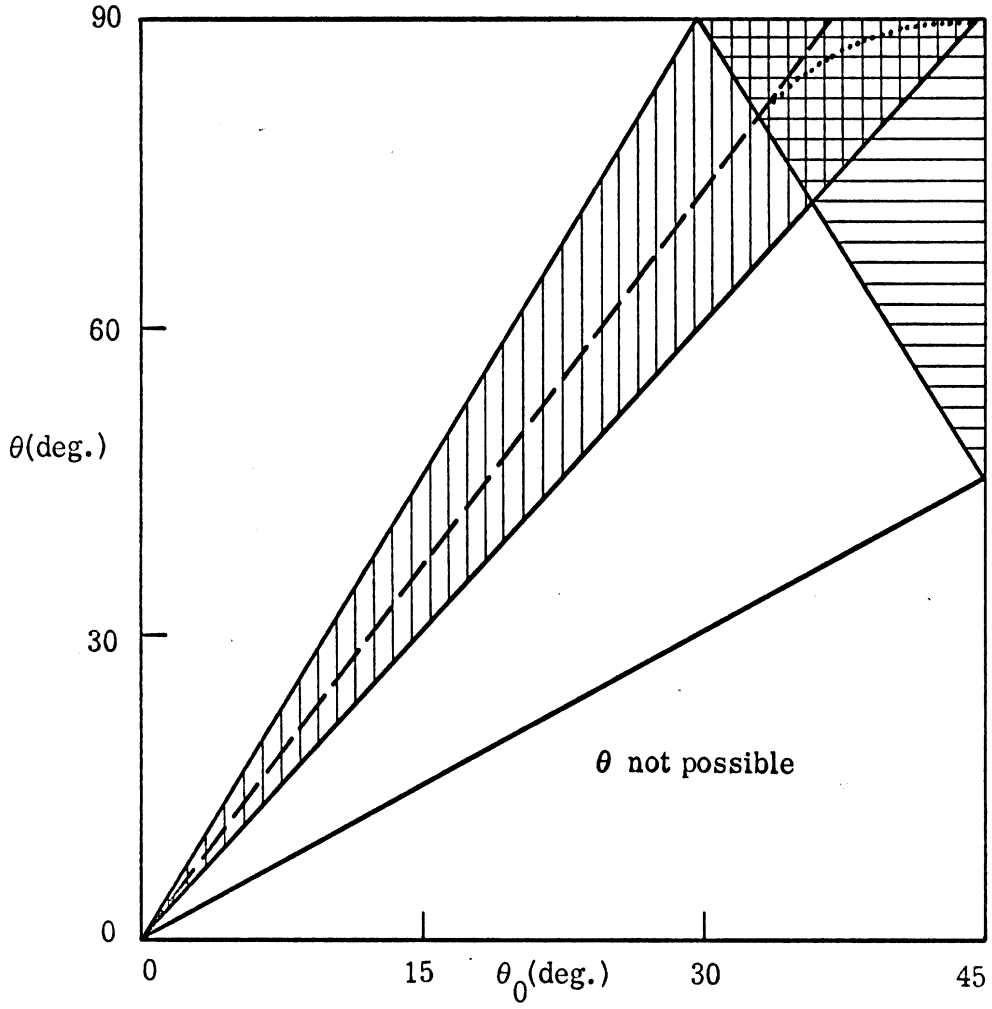

FIG. 5: THE SHADED REGIONS ARE THOSE WHERE REFLECTED WAVES CAN EXIST: $\nu_1 = 1$ IN THE HORIZONTALLY SHADED REGION AND $\nu_2 = 1$ IN THE VERTICALLY SHADED ONE; HOWEVER, IT IS NOT VALID TO INCLUDE REFLECTION OFF THE LOWER SURFACE OF THE CONE BELOW THE DOTTED LINE (SEE P. 35). ABOVE (BELOW) THE BROKEN LINE, THE TIME DELAY FOR THE RE-RADIATED CONTRIBUTION IS SHORTER (LONGER) THAN THAT FOR THE DOUBLY-DIFFRACTED ONE.

the field point P_0, and to measure time in nanoseconds. Since the velocity of light is, in MKS units, 3×10^8 m/sec = 0.3 m/nsec approximately, it follows that in all formulae from now on, c must be given the value 0.3 with distances measured in meters (of course). The time delays associated with the various diffraction contributions are now

$$t_1 = \frac{d}{c}\left\{1-\cos(\theta-\theta_0)\right\}\ , \qquad t_2 = \frac{d}{c}\left\{1+\cos(\theta+\theta_0)\right\}\ ,$$
$$t_3 = \frac{d}{c}\left\{1-\cos(\theta+3\theta_0)\right\}\ , \qquad t_4 = \frac{d}{c}\left\{1+\cos(\theta-3\theta_0)\right\}\ . \tag{68}$$

Observe that if $t_1 = t_1(\theta)$, we have

$$t_2 = t_1(\pi-\theta)\ , \qquad t_3 = t_1(2\pi-3\theta_0-\theta)\ , \qquad t_4 = t_1(\pi-3\theta_0+\theta)\ .$$

It is also convenient to normalize the fields by suppressing the factor $f_0/r\sin\theta$.

Using now the inverse Fourier transform (9), the time domain expression for the normalized electric field at the point P_0 when P_1 and P_2 are slope discontinuities is

$$E = U(t) + \frac{1}{\pi}\sqrt{\frac{c}{2d}\frac{\sin\theta}{\sin\theta_0}}\ \Big[D^s(\theta)(t-t_1)^{1/2}U(t-t_1)+D^s(\pi-\theta)(t-t_2)^{1/2}U(t-t_2)$$
$$+\nu_1 F(\theta)D^s(2\pi-2\theta_0-\theta)(t-t_3)^{1/2}U(t-t_3)$$
$$+\nu_2 F(\pi-\theta)D^s(\pi-2\theta_0+\theta)(t-t_4)^{1/2}U(t-t_4)\Big] \tag{69}$$

where $D^s(\theta)$ is given in Eq. (57). Similarly, for a discontinuity in curvature,

$$E = U(t) + \frac{1}{\pi}\sqrt{\frac{c}{2d}\frac{\sin\theta}{\sin\theta_0}}\ \Big[\tilde{D}^c(\theta)(t-t_1)^{3/2}U(t-t_1)+\tilde{D}^c(\pi-\theta)(t-t_2)^{3/2}U(t-t_2)$$
$$+\nu_1 F(\theta)\tilde{D}^c(2\pi-2\theta_0-\theta)(t-t_3)^{3/2}U(t-t_3)$$
$$+\nu_2 F(\pi-\theta)\tilde{D}^c(\pi-2\theta_0+\theta)(t-t_4)^{3/2}U(t-t_4)\Big] \tag{70}$$

where

$$\tilde{D}^c(\theta) = -\frac{2i\omega}{3} D^c(\theta)$$

and hence, from Eq. (59),

$$\tilde{D}^c(\theta) = -\frac{4ca_1}{3} \frac{1-\cos\theta_0\cos\left(\theta+\frac{\theta_0}{2}\right)}{\left\{\cos\theta_0-\cos\left(\theta+\frac{\theta_0}{2}\right)\right\}^3} \quad . \tag{71}$$

As we have previously remarked, the criteria for validity of an approximate solution in the frequency and time domains are somewhat different, and just because all four diffracted and diffracted-reflected contributions are of the same order in k does not imply that it is legitimate to include them in the time domain solution. An upper bound on the time duration for which our solution could be valid is provided by the shortest ray path whose contribution is omitted, and since we have not included any double diffraction or re-radiation contribution, a necessary condition for validity is

$$t < T \tag{72}$$

where

$$T = \frac{d}{c} \min. \left\{2,\ 1+2\cos\theta_0-\cos(\theta-\theta_0)\right\} \quad . \tag{73}$$

The angle θ for which

$$2 = 1+2\cos\theta_0-\cos(\theta-\theta_0) \tag{74}$$

is plotted as a function of θ_0, $\theta_0 \leq 45^\circ$, as a broken line in Fig. 5. Above this line

$$2 < 1+2\cos\theta_0-\cos(\theta-\theta_0)$$

so that the omission of any re-radiated contribution is now the more restrictive, whereas below the line

$$2 > 1+2\cos\theta_0-\cos(\theta-\theta_0) \ ,$$

making double diffraction the basis for our criterion. For $\theta_0 > 36.9^o$, Eq. (74) has no solution for $\theta \leq 90^o$.

For the contribution produced by diffraction at the lower surface singularity P_2 and then reflection off the upper surface of the cone, the associated time delay is t_4, and it can be verified that

$$t_4 \leq T$$

for all θ for which the path exists. At the lower boundary of the vertically shaded region in Fig. 5,

$$t_4 = \frac{d}{c}\left\{1+2\cos\theta_0-\cos(\theta-\theta_0)\right\} < \frac{2d}{c}$$

and at the upper boundary

$$t_4 = \frac{2d}{c} < \frac{d}{c}\left\{1+2\cos\theta_0-\cos(\theta-\theta_0)\right\} ,$$

and since $t_4 < T$ throughout the interior of the region, it is legitimate to include this contribution in our time domain solution.

The situation is rather different for the contribution which results from reflection off the lower surface of the cone. It is obvious that $t_3 \geq t_4$ with equality only for $\theta = 90^o$, and $t_3 \leq 2d/c$ with equality on the lower boundary of the horizontally shaded region in Fig. 5. Throughout most of this region, however, T is determined by the doubly diffracted ray, and $t_3 < T$ only at those points of the region lying <u>above</u> the dotted line in Fig. 5. For most practical purposes, therefore, this reflected ray contribution is of no interest in the time domain.

5. Data and Conclusions.

Expressions for the normalized transverse electric field E at a point (r,θ) in the far zone of the biconical portion of the antenna are given as functions of the elapsed time t in Eqs. (69) and (70). The first of these applies to the case of a cylindrical continuation which produces a slope discontinuity at the junction, and the second to a hyperbolic continuation for which the discontinuity is in curvature. Both are valid for only a short range of times, and a necessary (but not sufficient) condition for validity is that given in Eq. (72). In particular, it is required that

$$t < \frac{20}{3} d \tag{75}$$

where t is measured in nanoseconds and d in meters.

Each of the expressions for E(t) is valid for $0_0 < \theta \leq \pi/2$ and consists of a direct contribution from the source and up to four secondary contributions produced by diffraction and diffraction-reflection. All of the contributions are entirely real and since $D^s(\theta)$ and $\tilde{D}^c(\theta)$ are negative for $\theta_0 < \theta \leq \pi/2$, the secondary contributions subtract from the direct one. These properties are physically required. With increasing t, each secondary contribution increases as $(t-t_i)^{1/2}$ or $(t-t_i)^{3/2}$ according as the discontinuity is in slope or curvature respectively, where $t = t_i$ is the time of onset. Of necessity, there must now exist a time $t = t_i^*$ at which the secondary contributions are the same for the two geometries, all other parameters being equal. For $0 < t < t_i^*$, a discontinuity in curvature produces the smaller perturbation, whereas for $t > t_i^*$ a slope discontinuity is preferable. Each secondary contribution has its own associated "crossing time" t_i^* and there is obviously an analogous time t^* appropriate to the sum of all of them.

A knowledge of t^* in relation to the upper limit T of validity of our treatment is one of the key factors in assessing the relative merits of the two geometries. Unfortunately, t^* can in general be obtained only from an examination of computed data, but in the particular case where $\theta = \pi/2$ and the reflected contributions can be ignored,

$$t^* - t_1 = \frac{D^s(\pi/2)}{\tilde{D}^c(\pi/2)} \tag{76}$$

Hence, from Eqs. (57), (71) and (14),

$$t^* - t_1 = -\frac{3\epsilon d}{4c} \frac{2\lambda \sin\lambda\pi}{\cos\lambda\pi + \cos\frac{\lambda\pi}{2}} \frac{\left(\cos\theta_0 - \sin\frac{\theta_0}{2}\right)^3}{\sin 2\theta_0 \left(1 + \cos\theta_0 \sin\frac{\theta_0}{2}\right)} \tag{77}$$

showing an increase proportional to ϵ and d. By choosing ϵ large enough, we can ensure that the curvature discontinuity produces the smaller perturbation throughout the entire range of times $t < T$ for which our analysis is valid, and the value of ϵ for which $t^* = T$ has been computed from Eq. (77) and is plotted as a function of θ_0 in Fig. 6.

For values of θ other than $\pi/2$ it is necessary to turn to computed values of E(t) to draw any conclusions about the performance. A computer program has been written to calculate E(t) from Eqs. (69) and (70) for any combination of parameters. The program is quite straightforward and needs no comment, and in analyzing the data, the only complication is that produced by the number of parameters involved. The variation of the field strength with time is a function of θ, θ_0 and d and, in the case of a curvature discontinuity, of ϵ as well. Fortunately, however, the effect of some of these parameters is rather trivial. Thus, ϵ affects the perturbation produced by a curvature discontinuity only as a scaling factor: an increase in ϵ by a factor 2 decreases the perturbation by the same amount. The slant length d affects proportionally the times t_i at which the secondary contributions reach the field point (see Eqs. (68)) and, in addition, changes the magnitudes of all perturbations through a factor $d^{-1/2}$, but the dependence of E(t) on θ and θ_0 is much more involved.

The form of the computer output is illustrated in Tables 1 and 2 which show the normalized early time response, E(t), as a function of t for* $\theta \simeq 90^\circ$,

---

* $\epsilon = 0$ implies a slope discontinuity and, hence, Eq. (69), whereas $\epsilon \neq 0$ corresponds to a curvature discontinuity, i.e. Eq. (70).

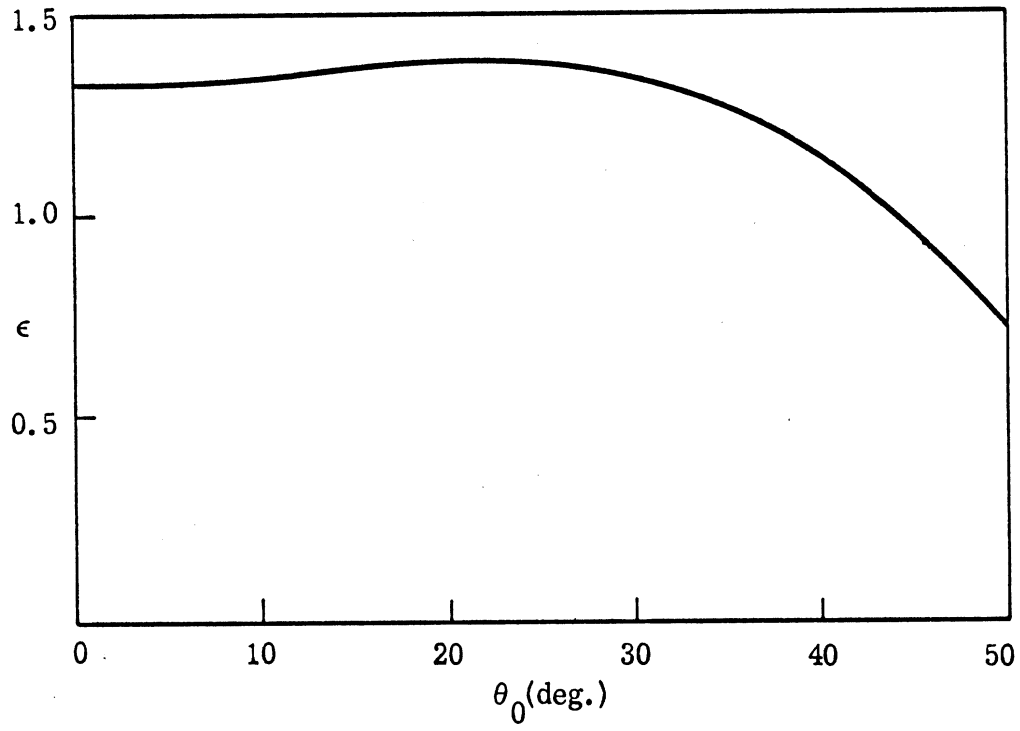

FIG. 6: THE FRACTIONAL INCREASE, ϵ, IN RADIUS FOR WHICH $t^* = T$ WHEN $\theta = 90^o$.

TABLE 1. Individual Contributions to E(t) for $\theta = 90^{o}$, $\theta_{o} = 30^{o}$, d = 1.5 m and $\epsilon = 0$.

TIME	TOTAL	LOWER DIF	UPPER DIF	LOWER REF	UPPER REF	SUB TOTAL
0.0	1.00	0.0	0.0	0.0	0.0	0.0
0.20	1.00	0.0	0.0	0.0	0.0	0.0
0.40	1.00	0.0	0.0	0.0	0.0	0.0
0.61	1.00	0.0	0.0	0.0	0.0	0.0
0.81	1.00	0.0	0.0	0.0	0.0	0.0
1.01	1.00	0.0	0.0	0.0	0.0	0.0
1.21	1.00	0.0	0.0	0.0	0.0	0.0
1.41	1.00	0.0	0.0	0.0	0.0	0.0
1.62	1.00	0.0	0.0	0.0	0.0	0.0
1.82	1.00	0.0	0.0	0.0	0.0	0.0
2.02	1.00	0.0	0.0	0.0	0.0	0.0
2.22	1.00	0.0	0.0	0.0	0.0	0.0
2.42	0.93	0.0	-0.07	0.0	0.0	-0.07
2.63	0.90	0.0	-0.10	0.0	0.0	-0.10
2.83	0.87	0.0	-0.13	0.0	0.0	-0.13
3.03	0.80	-0.06	-0.15	0.0	0.0	-0.20
3.23	0.75	-0.08	-0.17	0.0	0.0	-0.25
3.43	0.71	-0.11	-0.18	0.0	0.0	-0.29
3.64	0.68	-0.12	-0.20	0.0	0.0	-0.32
3.84	0.65	-0.14	-0.21	0.0	0.0	-0.35
4.04	0.62	-0.15	-0.22	0.0	0.0	-0.38
4.24	0.60	-0.16	-0.24	0.0	0.0	-0.40
4.44	0.58	-0.18	-0.25	0.0	0.0	-0.42
4.65	0.55	-0.19	-0.26	0.0	0.0	-0.45
4.85	0.53	-0.20	-0.27	0.0	0.0	-0.47
5.05	0.51	-0.21	-0.28	0.0	0.0	-0.49
5.25	0.49	-0.22	-0.29	0.0	0.0	-0.51
5.45	0.47	-0.23	-0.30	0.0	0.0	-0.53
5.66	0.46	-0.23	-0.31	0.0	0.0	-0.54
5.86	0.44	-0.24	-0.32	0.0	0.0	-0.56
6.06	0.42	-0.25	-0.33	0.0	0.0	-0.58
6.26	0.41	-0.26	-0.33	0.0	0.0	-0.59
6.46	0.39	-0.27	-0.34	0.0	0.0	-0.61
6.67	0.37	-0.27	-0.35	0.0	0.0	-0.63
6.87	0.36	-0.28	-0.36	0.0	0.0	-0.64
7.07	0.34	-0.29	-0.37	0.0	0.0	-0.66
7.27	0.33	-0.30	-0.37	0.0	0.0	-0.67
7.47	0.32	-0.30	-0.38	0.0	0.0	-0.68
7.68	0.30	-0.31	-0.39	0.0	0.0	-0.70
7.88	0.29	-0.31	-0.40	0.0	0.0	-0.71
8.08	0.28	-0.32	-0.40	0.0	0.0	-0.72
8.28	0.26	-0.33	-0.41	0.0	0.0	-0.74
8.48	0.25	-0.33	-0.42	0.0	0.0	-0.75
8.69	0.24	-0.34	-0.42	0.0	0.0	-0.76
8.89	0.22	-0.35	-0.43	0.0	0.0	-0.78
9.09	0.21	-0.35	-0.44	0.0	0.0	-0.79
9.29	0.20	-0.36	-0.44	0.0	0.0	-0.80
9.49	0.19	-0.36	-0.45	0.0	0.0	-0.81
9.70	0.18	-0.37	-0.46	0.0	0.0	-0.82
9.90	0.16	-0.37	-0.46	0.0	0.0	-0.84
10.10	0.13	-0.38	-0.47	-0.02	0.0	-0.87
10.30	0.11	-0.38	-0.47	-0.03	0.0	-0.89
10.51	0.09	-0.39	-0.48	-0.04	0.0	-0.91
10.71	0.07	-0.39	-0.49	-0.05	0.0	-0.93
10.91	0.05	-0.40	-0.49	-0.06	0.0	-0.95
11.11	0.03	-0.40	-0.50	-0.07	0.0	-0.97
11.31	0.02	-0.41	-0.50	-0.07	0.0	-0.98
11.52	-0.00	-0.41	-0.51	-0.08	0.0	-1.00
11.72	-0.02	-0.42	-0.51	-0.08	0.0	-1.02
11.92	-0.03	-0.42	-0.52	-0.09	0.0	-1.03
12.12	-0.05	-0.43	-0.53	-0.09	0.0	-1.05
12.32	-0.06	-0.43	-0.53	-0.10	0.0	-1.06
12.53	-0.07	-0.44	-0.54	-0.10	0.0	-1.07
12.73	-0.09	-0.44	-0.54	-0.10	0.0	-1.09
12.93	-0.10	-0.45	-0.55	-0.11	0.0	-1.10
13.13	-0.11	-0.45	-0.55	-0.11	0.0	-1.11
13.33	-0.13	-0.46	-0.56	-0.12	0.0	-1.13
13.54	-0.14	-0.46	-0.56	-0.12	0.0	-1.14
13.74	-0.15	-0.46	-0.57	-0.12	0.0	-1.15
13.94	-0.17	-0.47	-0.57	-0.13	0.0	-1.17
14.14	-0.18	-0.47	-0.58	-0.13	0.0	-1.18
14.34	-0.19	-0.48	-0.58	-0.13	0.0	-1.19
14.55	-0.20	-0.48	-0.59	-0.13	0.0	-1.20
14.75	-0.21	-0.48	-0.59	-0.14	0.0	-1.21
14.95	-0.23	-0.49	-0.60	-0.14	0.0	-1.23
15.15	-0.24	-0.49	-0.60	-0.14	0.0	-1.24
15.35	-0.25	-0.50	-0.61	-0.15	0.0	-1.25
15.56	-0.26	-0.50	-0.61	-0.15	0.0	-1.26
15.76	-0.27	-0.51	-0.61	-0.15	0.0	-1.27
15.96	-0.28	-0.51	-0.62	-0.15	0.0	-1.28

TABLE 2: Individual Contributions to E(t) for $\theta = 90^{o}$, $\theta_{o} = 30^{o}$, d = 1.5 m and $\epsilon = 1$.

TIME	TOTAL	LOWER DIF	UPPER DIF	LOWER REF	UPPER REF	SUB TOTAL
0.0	1.00	0.0	0.0	0.0	0.0	0.0
0.20	1.00	0.0	0.0	0.0	0.0	0.0
0.40	1.00	0.0	0.0	0.0	0.0	0.0
0.61	1.00	0.0	-0.00	0.0	0.0	-0.00
0.81	0.99	0.0	-0.01	0.0	0.0	-0.01
1.01	0.97	0.0	-0.03	0.0	0.0	-0.03
1.21	0.94	0.0	-0.06	0.0	0.0	-0.06
1.41	0.91	0.0	-0.09	0.0	0.0	-0.09
1.62	0.87	0.0	-0.13	0.0	0.0	-0.13
1.82	0.83	0.0	-0.17	0.0	0.0	-0.17
2.02	0.79	0.0	-0.21	0.0	0.0	-0.21
2.22	0.74	0.0	-0.26	0.0	0.0	-0.26
2.42	0.69	0.0	-0.31	0.0	0.0	-0.31
2.63	0.64	0.0	-0.36	0.0	0.0	-0.36
2.83	0.59	0.0	-0.41	0.0	0.0	-0.41
3.03	0.53	0.0	-0.47	0.0	0.0	-0.47
3.23	0.47	0.0	-0.53	0.0	0.0	-0.53
3.43	0.41	0.0	-0.59	0.0	0.0	-0.59
3.64	0.34	0.0	-0.66	0.0	0.0	-0.66
3.84	0.28	0.0	-0.72	0.0	0.0	-0.72
4.04	0.21	0.0	-0.79	0.0	0.0	-0.79
4.24	0.14	0.0	-0.86	0.0	0.0	-0.86
4.44	0.07	0.0	-0.93	0.0	0.0	-0.93
4.65	-0.01	0.0	-1.01	0.0	0.0	-1.01
4.85	-0.08	0.0	-1.08	0.0	0.0	-1.08
5.05	-0.16	0.0	-1.16	0.0	0.0	-1.16
5.25	-0.24	0.0	-1.24	0.0	0.0	-1.24
5.45	-0.32	-0.00	-1.32	0.0	0.0	-1.32
5.66	-0.41	-0.00	-1.41	0.0	0.0	-1.41
5.86	-0.50	-0.00	-1.49	0.0	0.0	-1.50
6.06	-0.59	-0.01	-1.58	0.0	0.0	-1.59
6.26	-0.68	-0.01	-1.67	0.0	0.0	-1.68
6.46	-0.77	-0.01	-1.76	0.0	0.0	-1.77
6.67	-0.87	-0.02	-1.85	0.0	0.0	-1.87
6.87	-0.96	-0.02	-1.94	0.0	0.0	-1.96
7.07	-1.06	-0.03	-2.03	0.0	0.0	-2.06
7.27	-1.16	-0.03	-2.13	0.0	0.0	-2.16
7.47	-1.26	-0.04	-2.23	0.0	0.0	-2.26
7.68	-1.37	-0.04	-2.33	0.0	0.0	-2.37
7.88	-1.47	-0.05	-2.43	0.0	0.0	-2.47
8.08	-1.58	-0.05	-2.53	0.0	0.0	-2.58
8.28	-1.69	-0.06	-2.63	0.0	0.0	-2.69
8.48	-1.80	-0.07	-2.73	0.0	0.0	-2.80
8.69	-1.91	-0.07	-2.84	0.0	0.0	-2.91
8.89	-2.03	-0.08	-2.95	0.0	0.0	-3.03
9.09	-2.14	-0.09	-3.05	0.0	0.0	-3.14
9.29	-2.26	-0.09	-3.16	0.0	0.0	-3.26
9.49	-2.38	-0.10	-3.27	0.0	0.0	-3.38
9.70	-2.50	-0.11	-3.39	0.0	0.0	-3.50
9.90	-2.62	-0.12	-3.50	0.0	0.0	-3.62
10.10	-2.74	-0.12	-3.61	0.0	0.0	-3.74
10.30	-2.86	-0.13	-3.73	0.0	0.0	-3.86
10.51	-2.99	-0.14	-3.85	0.0	0.0	-3.99
10.71	-3.11	-0.15	-3.97	0.0	0.0	-4.11
10.91	-3.24	-0.16	-4.09	0.0	0.0	-4.24
11.11	-3.37	-0.17	-4.21	0.0	0.0	-4.37
11.31	-3.50	-0.17	-4.33	0.0	0.0	-4.50
11.52	-3.63	-0.18	-4.45	0.0	0.0	-4.63
11.72	-3.77	-0.19	-4.57	0.0	0.0	-4.77
11.92	-3.90	-0.20	-4.70	0.0	0.0	-4.90
12.12	-4.04	-0.21	-4.83	0.0	0.0	-5.04
12.32	-4.17	-0.22	-4.95	0.0	0.0	-5.17
12.53	-4.31	-0.23	-5.08	0.0	0.0	-5.31
12.73	-4.45	-0.24	-5.21	0.0	0.0	-5.45
12.93	-4.59	-0.25	-5.34	0.0	0.0	-5.59
13.13	-4.73	-0.26	-5.47	0.0	0.0	-5.73
13.33	-4.88	-0.27	-5.61	0.0	0.0	-5.88
13.54	-5.02	-0.28	-5.74	0.0	0.0	-6.02
13.74	-5.17	-0.29	-5.87	0.0	0.0	-6.17
13.94	-5.31	-0.30	-6.01	0.0	0.0	-6.31
14.14	-5.46	-0.31	-6.15	0.0	0.0	-6.46
14.34	-5.61	-0.32	-6.29	0.0	0.0	-6.61
14.55	-5.76	-0.33	-6.42	0.0	0.0	-6.76
14.75	-5.91	-0.34	-6.56	0.0	0.0	-6.91
14.95	-6.06	-0.36	-6.71	0.0	0.0	-7.06
15.15	-6.21	-0.37	-6.85	0.0	0.0	-7.21
15.35	-6.37	-0.38	-6.99	0.0	0.0	-7.37
15.56	-6.52	-0.39	-7.13	0.0	0.0	-7.52
15.76	-6.68	-0.40	-7.28	0.0	0.0	-7.68
15.96	-6.84	-0.41	-7.43	0.0	0.0	-7.84

$\epsilon = 0$ and $\theta \simeq 60^{\circ}$, $\epsilon = 1$, the other parameters being the same ($d = 1.5$ m, $\theta_0 \simeq 30^{\circ}$). The total field is broken down into its various components and the last column (labelled "sub-total") is just the sum of the four previous columns, i.e. the net perturbation. Although $T \simeq 10$ nsec for both Tables, we have included data for times up to 16 nanoseconds to demonstrate the increasingly negative value of the field amplitude as t increases. Indeed, as $t \rightarrow \infty$, $E(t) \rightarrow -\infty$, but this is just a consequence of the failure of the initial time approximation. As noted earlier and evident in Table 1, the reflected field for $\theta = 90^{\circ}$ comes in just before the limit of allowable times and only achieves a significant magnitude at times which are greater than those that can be entertained. For values of θ markedly less than 90°, the same conclusion holds for the diffracted contribution of the lower discontinuity (see Table 2). Thus, for most practical purposes, it is sufficient to ignore any contribution due to reflection, i.e. put $\nu_1 = \nu_2 = 0$ in Eqs. (69) and (70) for all θ and θ_0, and, in addition, include only one diffracted contribution when θ differs markedly from 90°.

The effect of changing from the slope to a curvature discontinuity is illustrated in Fig. 7 for the case in which $d = 1.5$ m, $\theta_0 = 29^{\circ}$, $\theta = 90^{\circ}$ and $\epsilon = 1$. The crossing time t^* is 8.3 nsec, which is not far short of the limit $T = 10$ nsec for which the solutions are admissible. As judged by the magnitude of the field perturbation, this particular curvature discontinuity is superior to the slope discontinuity over most of the admissible time span, and to increase ϵ or d enhances this superiority. When $\theta = 90^{\circ}$, the contributions from the upper and lower bicones and discontinuities come in at the same time, but this is not true for $\theta \neq 90^{\circ}$. This is illustrated in Figs. 8 and 9. In both cases $d = 3.0$ m and the curves are for a slope discontinuity ($\epsilon = 0$) and a curvature discontinuity having $\epsilon = 1$. In Fig. 8, $\theta = 75^{\circ}$ and $\theta_0 = 35^{\circ}$ for which the maximum allowable time is $T = 18.7$ nsec. The breakpoints associated with the two diffracted contributions are clearly differentiated and even the contribution due to reflection off the lower bicone enters within the allowable time span, as predicted by Fig. 5. The curve for the curvature discontinuity has these same breakpoints, though they are not so immediately apparent.

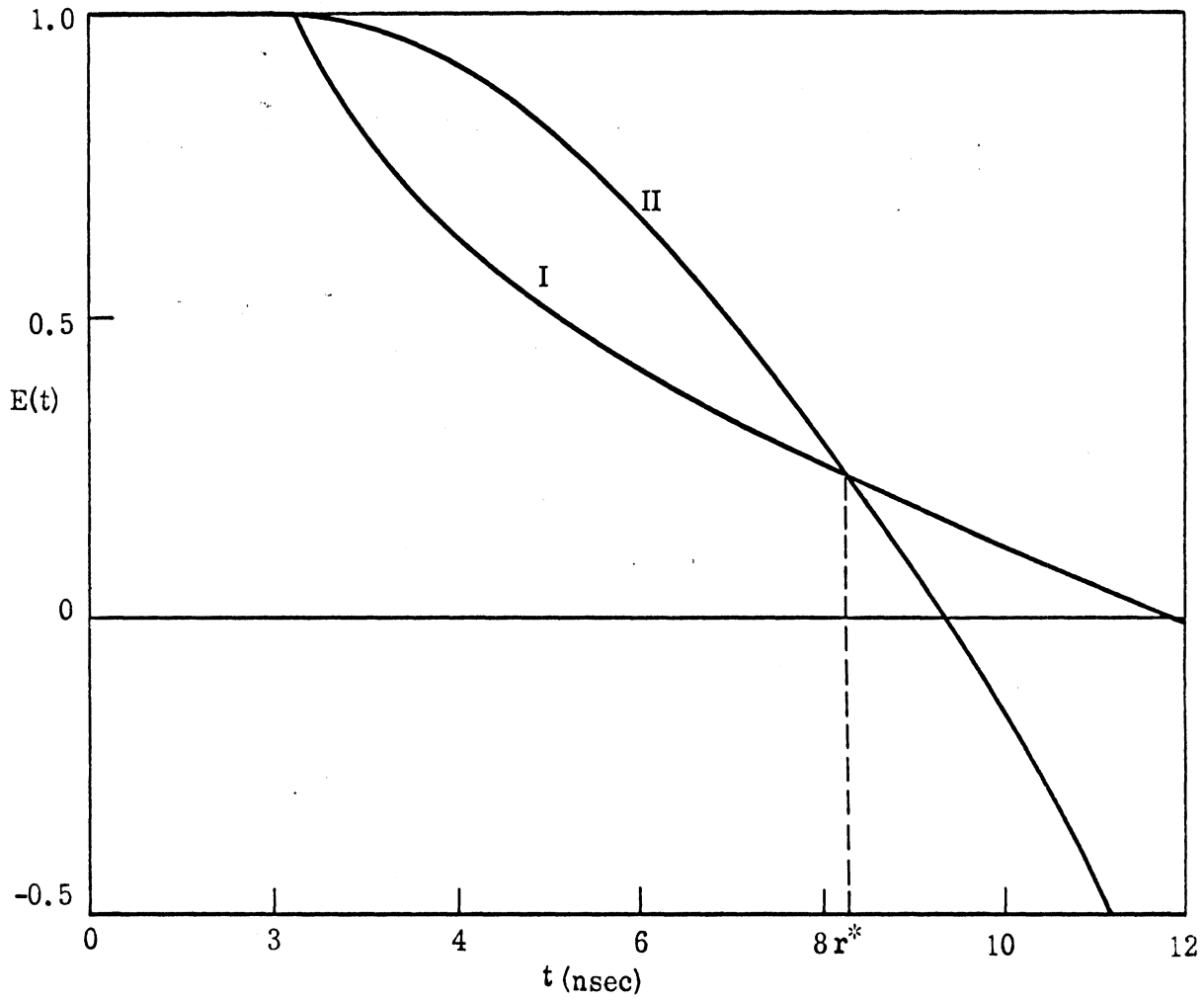

FIG. 7: NORMALIZED ELECTRIC FIELD E(t) FOR SLOPE (I) AND CURVATURE (II: $\epsilon = 1$) DISCONTINUITIES WITH $\theta = 90^{\circ}$, $\theta_0 = 29^{\circ}$ AND d = 1.5 m.

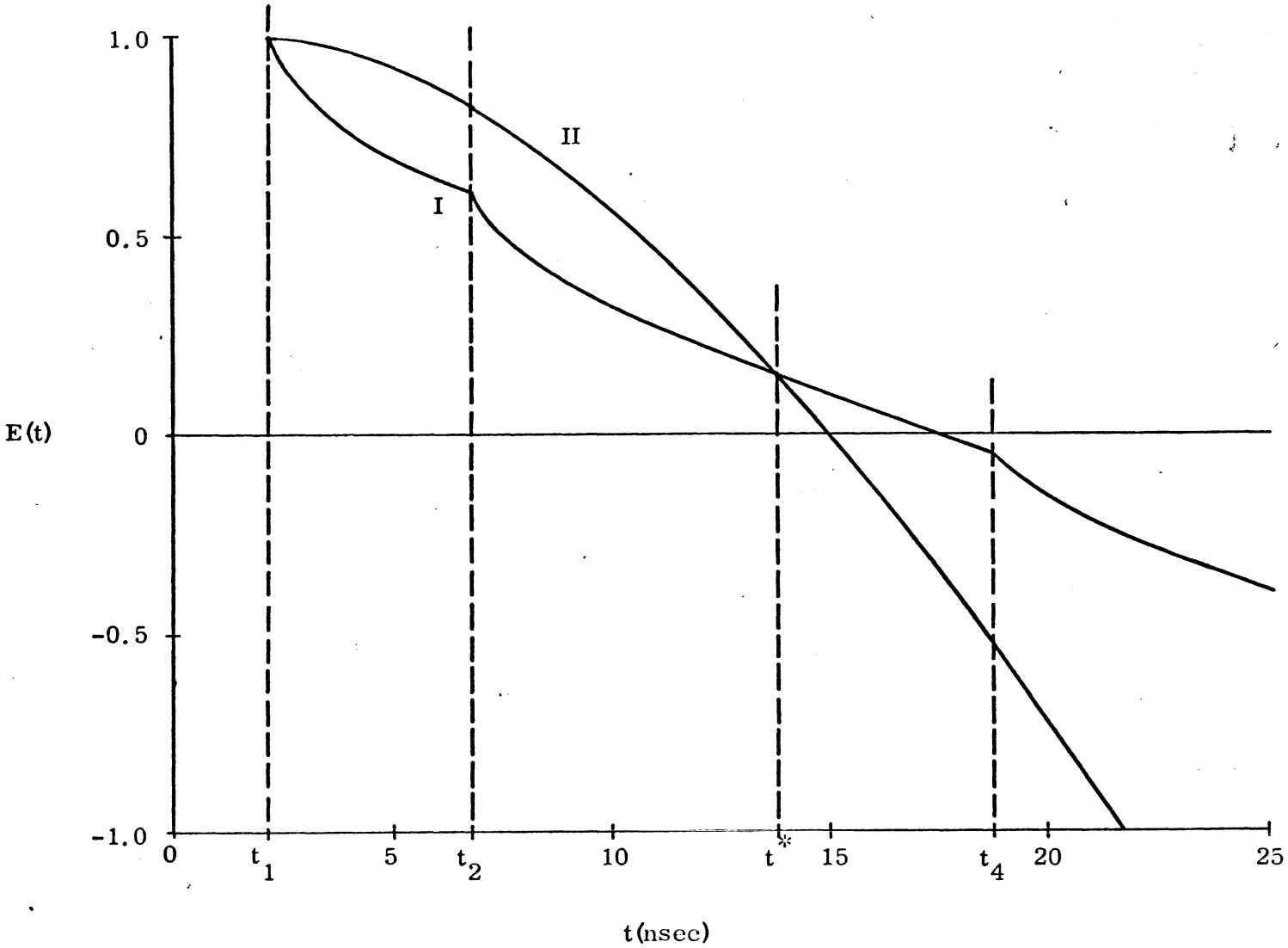

FIG. 8: NORMALIZED ELECTRIC FIELD E(t) FOR SLOPE (I) AND CURVATURE (II: $\epsilon = 1$) DISCONTINUITIES WITH $\theta = 75^o$, $\theta_0 = 35^o$ AND d = 3.0 m.

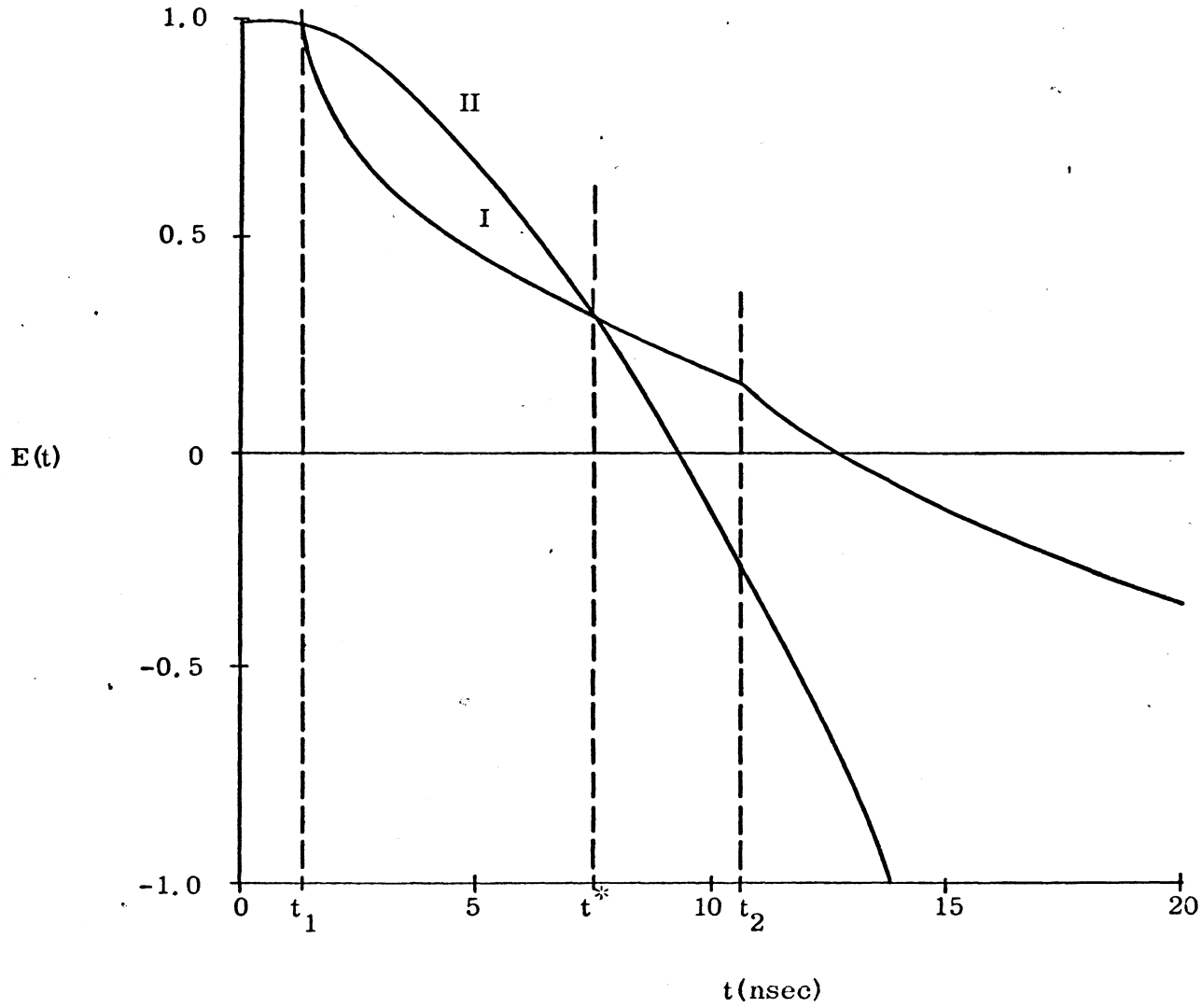

FIG. 9: NORMALIZED ELECTRIC FIELD E(t) FOR SLOPE (I) AND CURVATURE (II: $\epsilon = 1$) DISCONTINUITIES WITH $\theta = 57^{\circ}$, $\theta_0 = 29^{\circ}$ AND d = 3.0 m.

The effect of decreasing θ and 0^o to 57^o and 29^o respectively is illustrated in Fig. 9. Observe that the crossing time t^* is now 7.5 nsec which is less than half of the allowable time span T = 18.7 nsec, whereas in Fig. 8, t^* = 13.9 nsec. By and large, t^* varies little with θ_0 but decreases uniformly with decreasing θ. This is evident from Table 3 where crossing times are listed for d = 1.5 m, ϵ = 1 and a variety of θ and θ_0. Since T does not differ drastically from 10 nsec for all of these θ and θ_0, it is apparent that for $\theta < 66^o$ the curvature discontinuity is better for less than 50 percent of the allowable times; and we note that when it is worse, it is much, much worse, because of the slope of the time domain curves (see Figs. 7-9).

So far we have compared the performance of antennas whose bicones are identical in size and shape, but which differ in the form of the continuation

TABLE 3:

t^* AS A FUNCTION OF θ AND θ_0 FOR d = 1.5m AND ϵ = 1

θ \ θ_0	15	20	25	30	35	40
90	8.27	8.13	8.05	8.02	8.08	8.28
87	7.83	7.70	7.62	7.60	7.68	7.88
84	7.39	7.27	7.19	7.18	7.27	7.49
81	6.95	6.84	6.77	6.77	6.86	7.09
78	6.52	6.41	6.35	6.35	6.46	6.70
75	6.09	5.99	5.93	5.94	6.06	6.32
72	5.66	5.57	5.52	5.52	5.67	5.95
66	4.84	4.75	4.72	4.76	4.91	5.25
60	4.05	3.98	3.96	4.02	4.21	4.64
54	3.32	3.25	3.25	3.34	3.61	4.21

structure. This is not the only possible comparison. When the cone is mated to a cylinder of constant radius, creating a slope discontinuity at the junction, the final radius of the antenna is simply the radius of the ring discontinuity, i.e. $d \sin \theta_0$. On the other hand, to match the slopes, leaving a discontinuity in curvature, necessarily increases the maximum radius of the antenna, and in the particular case where the continuation has the hyperbolic profile (12), the final radius is the maximum radius, namely $(1+\epsilon) d \sin \theta_0$. It can now be argued that practical considerations limit the maximum radius of the antenna, and that a legitimate comparison between the two types of antenna should be based on this radius rather than the radius of the ring discontinuity. When this is done, the superiority of the hyperbolic continuation is far from overwhelming.

Such a comparison is illustrated in Table 4 for antennas having a half-cone angle $\theta_0 \simeq 29^\circ$. For antennas with a slope discontinuity, three different values

TABLE 4

d	θ	ϵ	Final Radius	Time (nsec) 4	6	8	10
1.0	90°	0	.5	.43	.22	-.04	-.23
.5	90°	1	.5	-.69	-2.7	-5.2	-8.1
.33	90°	2	.5	-.88	-2.87	-5.3	-8.1
2.0	90°	0	1.0	.81	.57	.43	.31
1.0	90°	1	1.0	.63	.06	-.69	-1.62
.66	90°	2	1.0	.52	-0.9	-.88	-1.82
3.0	90°	0	1.5	1.0	.81	.63	.52
1.5	90°	1	1.5	.90	.63	.27	-.16
1.0	90°	2	1.5	.82	.53	.16	-.31
3.0	60°	0	1.5	.55	.41	.29	.20
1.5	60°	1	1.5	.22	-.56	-1.54	-2.68
1.0	60°	2	1.5	.59	.34	.09	-.16

$\theta_0 = .51$ rad.

of d are considered and the response noted at t = 4, 6, 8 and 10 nsec. Each antenna is compared with two having curvature discontinuities at slant distances $d/(1+\epsilon)$ which are such as to yield the same overall antenna radius. The more the response differs from 1.0, the greater the field perturbation and (for our purposes) the poorer the antenna. As judged by the responses at the times listed in Table 4, each of the curvature-discontinuity antennas is substantially inferior to the equivalent slope-discontinuity one.

This conclusion, however, is not entirely fair on several counts. To change d changes the time T beyond which the analysis is invalid, and thus, when $d = 1.0$ and $\epsilon = 1$, $T = 6.66$ nsec, but when $d = 0.5$ and 0.33, $T = 3.33$ and 2.22 nsec respectively. Hence, as regards the first three lines in Table 4, the comparison with the curvature-discontinuity antennas has been made at times far beyond the limits of applicability for these antennas. The same criticism applies to most of the other comparisons in the Table. On the other hand, had we concentrated on the responses at sampled times such as 1, 2, 3 nsec to ensure the validity of the comparison, it would have been found that in almost all cases, the slope-discontinuity antenna had a response of 1.0, showing no perturbation at all, since the first diffracted contribution would not yet have arrived. Once again, the curvature-discontinuity antennas would have been judged inferior, albeit by not so large an amount.

A more fundamental criticism of the comparison is possible. We have already remarked that the hyperbolic continuation is only one of many serving to match the slope of the bicone. Others can be found which achieve the same purpose but yield different values for the maximum radius of the antenna. In practice, it is not even necessary that the continuation profile be a single analytic curve, and having followed (say) a hyperbolic profile for some distance beyond the upper limit of the cone, a different profile function can be introduced. Provided the new singularity which is created lies well within the shadow region, it could even take the form of a discontinuity in slope without substantially affecting the early time behavior. All such geometries require a much smaller (fractional) increase in the radius of the antenna than is implied by (14) for the same discon-

tinuity in curvature, although some increase beyond that of the slope-discontinuity antenna is inevitable.

By its very nature, a discontinuity in curvature produces a smaller amount of high frequency diffraction than a discontinuity in slope and hence, all other factors being equal, the former is preferable as regards the early time behavior of the antenna. The analysis we have given enables the effects to be determined, but whether the improvement is sufficient to compensate for the increased radium and difficulty of construction of the antenna, is a topic beyond the perview of this report.

References

Fock, V.A. (1965), Electromagnetic diffraction and propagation problems, Pergamon Press, New York.

Hong, S. and V.H. Weston (1966), A modified Fock function for the distribution of currents in the penumbra region with discontinuity in curvature, Radio Sci. 1, 1045-1053.

Kay, I. and J.B. Keller (1954), Asymptotic evaluation of the field at a caustic, J. Appl. Phys. 25, 876-883.

Keller, J.B. (1957), Diffraction by an aperture, J. Appl. Phys. 28, 426-444.

Keller, J.B. (1962), Geometrical theory of diffraction, J. Opt. Soc. Amer. 52, 116-130.

Sancer, M.I. and A.D. Varvatsis (1971), Geometrical diffraction solution for the high frequency - early time behavior of the field radiated by an infinite cylindrical antenna with a biconical feed, Sensor and Simulation Notes No. 129.

Senior, T.B.A. (1971), The diffraction matrix for a discontinuity in curvature, Sensor and Simulation Notes No. 132.

Senior, T.B.A. (1972), Divergence factors, University of Michigan Radiation Laboratory Memorandum No. 010748-504-M.

Senior, T.B.A. and P.L.E. Uslenghi (1971), High-frequency backscattering from a finite cone, Radio Sci. 6, 393-406.

Weston, V.H. (1965), Extension of Fock theory for currents in the penumbra region, Radio Sci. 69D, 1257-1270.